https://doi.org/10.5194/hess-2023-146
Preprint. Discussion started: 11 July 2023

Hydrology and Earth System Sciences
Discussions

Unraveling phenological responses to extreme drought and implications for water and carbon budgets

Nicholas K. Corak[1,2], Jason A. Otkin[3], Trent W. Ford[4], and Lauren E. Lowman[1,2]

[1]Department of Physics, Wake Forest University, Winston-Salem, NC, USA
[2]Department of Engineering, Wake Forest University, Winston-Salem, NC, USA
[3]Cooperative Institute for Meteorological Satellite Studies, Space Science and Engineering Center, University of Wisconsin-Madison, Madison, WI, USA
[4]Illinois State Water Survey, Prairie Research Institute, University of Illinois at Urbana-Champaign, Urbana-Champaign, IL, USA

Correspondence: Lauren E. L. Lowman (lowmanle@wfu.edu)

Abstract. In recent years, extreme drought events in the United States have seen increases in frequency and severity underlining a need to improve our understanding of vegetation resilience and adaptation. Flash droughts are extreme events marked by rapid dry down of soils due to lack of precipitation, high temperatures, and dry air. These events are also associated with reduced preparation, response, and management time windows before and during drought which exacerbate their detrimental impacts on people and food systems. Improvements in actionable information for flash drought management are informed by atmospheric and land surface processes, including responses and feedbacks from vegetation. Phenologic state, or growth stage, is an important metric for modeling how vegetation interacts with the atmosphere. We investigate how uncertainty in vegetation phenology propagates through vegetation responses during drought and non-drought periods by coupling a land-surface hydrology model to a predictive phenology model. We identify plant processes that influence vegetation responses to drought and assess the role of vegetation in the partitioning of carbon, water, and energy fluxes. We selected study sites in Kansas, USA where extreme drought events have been observed, in particular the flash drought of 2012, and where AmeriFlux eddy covariance towers provide data which can be used to evaluate water movement between the land (surface and subsurface) and the atmosphere. We evaluate the evolution of plant phenology, water use, and productivity using different water stress events. Results show that phenological responses using model parameters generated from periods of average precipitation show slower responses to drought as compared to parameters generated to reflect isohydric or anisohydric tendencies. Evapotranspiration (ET) and gross primary productivity (GPP) show similarly timed responses to water stress. We find plants alter water use strategies under extreme drought, with plants nearly halting atmospheric water and carbon exchanges when under stress. Decreases in uncertainty from ensemble estimates of GPP and ET during the flash drought period reduce to winter levels implying variability in plant life stage and functionality during drought periods are similar to those of dormant months. These results have implications for improving predictions of drought impacts on vegetation.

https://doi.org/10.5194/hess-2023-146
Preprint. Discussion started: 11 July 2023


Hydrology and Earth System Sciences
Discussions

1 Introduction

Frequency and severity of extreme droughts are predicted to increase within the next century (Dai, 2013). Flash droughts are a particular type of extreme drought characterized by their rapid intensification (Svoboda et al., 2002; Ford and Labosier, 2017; Otkin et al., 2018, 2022). The flash drought of 2012 that impacted the Central United States amplified the need to understand and predict flash droughts because of its estimated $30 billion of impacts to agriculture (Otkin et al., 2018). Work over the last decade has improved methods for identifying flash droughts based on development time and concurrent meteorological conditions (see Lisonbee et al., 2021, for a summary of flash drought definitions and indicators). Many studies have examined the drivers (e.g., lack of precipitation, greater atmospheric demand for water, above average temperatures) and impacts (e.g., soil moisture deficits and damages to agriculture) of flash drought (e.g., Lowman et al., in press; Christian et al., 2023, 2022; Jin et al., 2019; Otkin et al., 2018) while others have examined vegetation-atmosphere interactions (Chen et al., 2021; Zhang and Yuan, 2020; Gerken et al., 2018; Otkin et al., 2016; Novick et al., 2016).

Further assessment of vegetation-atmosphere feedback mechanisms may help improve identification of flash drought onset (Qing et al., 2022). Gross primary productivity (GPP), or carbon assimilation by plants during photosynthesis, is one such vegetation-atmospheric interaction. Large reductions in GPP due to soil moisture and temperature anomalies can be used to mark the beginning and duration of flash drought events (Zhang and Yuan, 2020; Poonia et al., 2022), as seen in the 2012 flash drought (Jin et al., 2019). Flash droughts can intensify through land-atmosphere feedbacks (Basara et al., 2019); for example, vegetation expediting water stress by pulling water from deeper soil layers and further drying soils (Qing et al., 2022). Otkin et al. (2016) studied the evolution of soil moisture and vegetation conditions during the 2012 event, finding that changes in soil moisture and evaporative stress indicators preceded rapid drought intensification in the US Drought Monitor (USDM, Svoboda et al. (2002)). Chen et al. (2019) found declines in evapotranspiration (ET), another interaction between the vegetation and the atmosphere, to be a major sign of flash drought intensification.

Interactions between vegetation and the atmosphere are altered during flash drought events, thus it is necessary to consider vegetation state when studying the effects of flash drought (Chen et al., 2021). Additionally, capturing differences across plant types is essential for modeling vegetation response to drought. Failure to account for differential responses across plant function types (PFTs) could result in underestimating the plant's ability to maintain its function under water stress (Zhou et al., 2013). Roman et al. (2015) showed that tree species in a forested region behaved differently during drought, with some species exhibiting isohydric tendencies, whereas others were more anisohydric. Isohydric plants are more conservative with their water use strategies when under stress and tend to regulate their stomatal conductance making them less susceptible to hydraulic failure (Konings and Gentine, 2017). These tendencies dictate how much photosynthesis occurs and thus how much carbon is exchanged (Roman et al., 2015). However, Garcia-Forner et al. (2017) cautions against making links between carbon assimilation and water potential regulation by showing similar rates of carbon assimilation under controlled drought simulations between two species of Mediterranean trees with opposing drought responses (one isohydric and one anisohydric). For some species, hydraulic regulation exists on a spectrum and can shift between isohydric and anisohydric in response to atmospheric and water conditions (Guo et al., 2020; Wu et al., 2021) leading to variation and uncertainties in water use

https://doi.org/10.5194/hess-2023-146
Preprint. Discussion started: 11 July 2023


Hydrology and Earth System Sciences
Discussions

strategies (Kannenberg et al., 2022). Ecosystem scale modeling may be able to incorporate the plant level spatial and temporal variability in water use strategies (Kannenberg et al., 2022) by taking into account concurrent meteorological and environmental conditions that influence plant water use tendencies beyond the species physiological characteristics (Hochberg et al., 2018).

Vegetation state parameterization in ecohydrological models could also dictate whether an area experiences carbon uptake changes during a flash drought due to the linkage between ET and GPP that couples the carbon and water cycles (Hosseini et al., 2022). There is evidence connecting vegetation changes in response to flash drought to lower plant production (Zhang et al., 2020; Jin et al., 2019; He et al., 2018; Otkin et al., 2016; Hunt et al., 2014). Jin et al. (2019) and He et al. (2018) found that croplands, grasslands, and shrublands experienced the majority of loss to carbon uptake rates during the droughts of 2011 and 2012 across the central US and similar rates of ET were found in croplands in the US northern plain flash drought of 2017 (He et al., 2019; Kimball et al., 2019). Chen et al. (2021) showed increases in LAI led to increased ET and that in a low moisture regime the amount of latent heat released due to ET was sensitive to changes in LAI. Hunt et al. (2014) showed that maize experienced decreases in stomatal conductance, which led to declines in GPP and ET, during a flash drought. Multiple studies showed crop yield losses following flash drought (e.g., Otkin et al., 2016; Hunt et al., 2014).

Previous studies have used remotely sensed or ground measurements and indicators to study vegetation responses to flash drought (e.g., Christian et al., 2022; Zhang et al., 2020; Basara et al., 2019). In contrast, Chen et al. (2021) used an earth system model to gauge plant behavior during flash drought while Hosseini et al. (2022) used models with different phenological forcing to investigate impacts on the water and carbon cycles during drought. Remotely sensed and eddy covariance data provide snapshots of the state of the system at point or preset spatial resolutions, and fixed temporal resolutions, while models can scale in space and time. Inherently simplified due to the complexity of systems, numerical models incorporate physical and biological processes and statistical techniques to make predictions based on current states and their uncertainties (Dietze, 2017). Data assimilation procedures and Bayesian inference allow modelers to incorporate observations while also identifying sources of uncertainty in both processes and scale (Dietze et al., 2013; Dietze, 2017).

Capturing phenology has implications for photosynthetic activity (Lowman and Barros, 2018; Stöckli et al., 2008; Jolly et al., 2005) which will influence the water, carbon, and energy fluxes coupled between the land and atmosphere. We use two versions of the Duke Coupled Land-Surface Hydrology Model (DCHM) that incorporate physically parameterized routines for photosynthesis (Garcia-Quijano and Barros, 2005; Gebremichael and Barros, 2006) and predictive phenology, or plant life stage (Lowman and Barros, 2016, 2018) to more closely investigate if and how vegetation water use strategies accelerate or decelerate dry down before and during flash drought. Data assimilation techniques allow us to capture model uncertainty around processes controlling vegetation activity, and in particular, assimilating vegetation phenology can improve the detection of drought (Mocko et al., 2021). We investigate whether plants exhibit anisohydric tendencies thereby exacerbating the dry down, or whether they regulate their water intake to preserve soil moisture to mitigate the effects of flash drought. In turn, we also investigate if plant behavior can be altered during periods of water stress by predicting phenology model parameters from hydrologic model outputs in dry and wet periods. We hypothesize that simulated transpiration and carbon uptake rates will taper during flash drought due to limited soil water availability and that the phenological changes are directly related to changes in transpiration rates and GPP (Figure 1). Our specific hypotheses are:

https://doi.org/10.5194/hess-2023-146
Preprint. Discussion started: 11 July 2023

Hydrology and Earth System Sciences
Discussions
Open Access
EGU

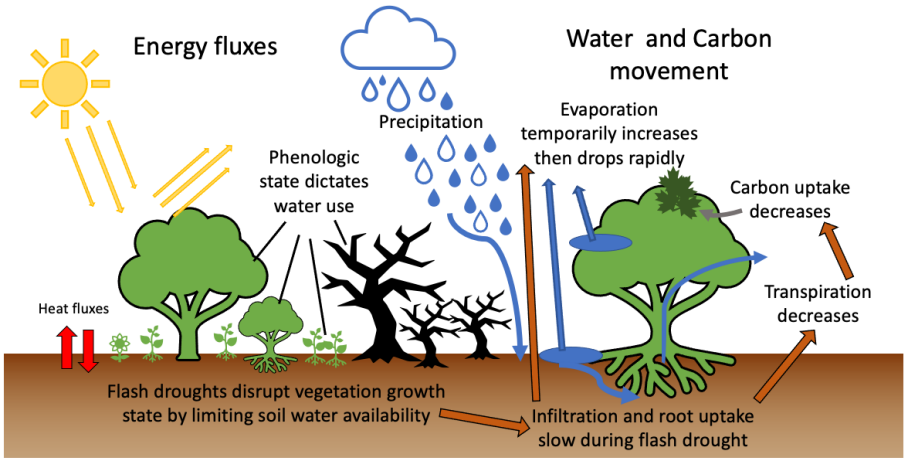

Figure 1. Schematic of water, carbon, and energy fluxes with hypotheses about ecological responses to flash drought indicated with orange arrows. Evaporation initially increases before completely shutting down due to lack of precipitation and increased atmospheric demand for water. Water will also evaporate shortly after precipitation events leaving little to no chance of infiltration. Infiltration and root-uptake slow during flash drought causing declines in rates of transpiration and carbon uptake. In response to decreases in water availability, vegetation phenological states will diminish exacerbating the reduction in plant-atmosphere interactions.

H1 Evaporation initially increases before completely shutting down due to lack of precipitation and increased atmospheric demand for water. Water will also evaporate shortly after precipitation events leaving little to no chance of infiltration.

H2 Infiltration and root-uptake slow during flash drought causing declines in rates of transpiration and carbon uptake.

H3 In response to decreases in water availability, vegetation phenological states will diminish exacerbating the reduction in plant-atmosphere interactions.

Here we use phenological responses, (i.e., FPAR, LAI) to examine how flash droughts affect vegetation state and ultimately impact the surface fluxes governing the movement of water and carbon between the land and atmosphere. We use the well-studied flash drought of 2012 to compare vegetation growth state and water use strategies during flash drought and non-drought periods to better understand how plants modulate water and interact with the atmosphere when under stress. We compare our model results with eddy covariance and remotely sensed values of vegetation state and atmospheric interactions. Discrepancies between observations and models with predictive versus forced phenology illuminate physical processes dictating plant water use strategies, for example, suppressing transpiration by closing stomata and limiting carbon intake. This study extends previous research on the water and carbon movement between plants and the atmosphere during flash drought by simulating the propagation of uncertainty after implementing a predictive phenology routine to understand how variability in the representation of vegetation state within a modeling framework impacts land-atmosphere exchanges during extreme drought events.

https://doi.org/10.5194/hess-2023-146
Preprint. Discussion started: 11 July 2023


Hydrology and Earth System Sciences
Discussions

2 Methods and Data

2.1 Overview of Modeling Approach

Remotely sensed or ground observations of land and atmospheric responses to flash drought are useful in identifying changes in plant phenology, soil moisture, evaporation rates, etc., but observations alone are unable to fully explain the mechanisms driving the ecological responses and water use strategy adaptations. Physically-based models can help fill the gaps in understanding what drives these changes by identifying key processes in the land-atmosphere interactions. For example, decreases in ground-based or satellite-derived GPP do not illuminate what processes caused the change, whereas a process based model might be able to signal that changes in root water uptake lead to decreased transpiration rates, which ultimately lead to decreased photosynthesis and carbon assimilation.

Within physical models, changes in state variables (e.g., soil moisture, root uptake, evaporation rates, etc.) are dependent upon forced meteorological conditions. Water use strategies are dictated by vegetation phenological states (Hu et al., 2008) and strongly influence GPP and ET (Beer et al., 2009). Therefore, physical, process-based models are able to adapt to changing meteorological conditions and capture mechanistic changes in vegetation-atmosphere interactions. Our goal is to identify vegetation responses that occur as a result of flash drought and associate those changes with the physical parameterizations used in a land-surface hydrology model.

In order to identify physical mechanisms driving plant responses to flash drought intensification, we use the physically based Duke Coupled surface-subsurface Hydrology Model with dynamic vegetation (DCHM-V). We provide the DCHM-V with plant life stage updates from Moderate Resolution Imaging Spectroradiometer (MODIS) fraction photosynthetically active radiation (FPAR) and LAI products in order to establish baseline outputs of soil moisture (SM), root uptake (RU), ET, and GPP from the DCHM-V. We then implement an ensemble Kalman filter (EnKF) data assimilation procedure following Lowman and Barros (2018) to establish ensembles of parameters to use in a dynamic canopy biophysical properties (DCBP) model within the DCHM-V yielding the DCHM with prognostic vegetation (DCHM-PV). The prognostic vegetation (i.e. phenological) model uses seasonal parameters (e.g. temperature and photoperiod) as well as meteorological parameters (e.g., soil and atmospheric water availability) to predict vegetation state and functionality (e.g., Lowman and Barros, 2018; Kim et al., 2015; Caldararu et al., 2014; Stöckli et al., 2008; Moradkhani et al., 2005). In addition to recomputing the same outputs of interest from the DCHM-V, we run Monte Carlo simulations of the DCHM-PV with the ensemble parameters from the EnKF in order to predict FPAR and LAI from the DCBP rather than forcing phenology with MODIS. We validate model simulations against ground, remotely sensed, and other modeled observations. The data sets to force or validate all versions of the DCHM are summarized in Table 1 and described in the following subsections.

https://doi.org/10.5194/hess-2023-146
Preprint. Discussion started: 11 July 2023


Hydrology and Earth System Sciences
Discussions
Open Access
EGU

Table 1. Summary of data products and uses

Dataset	Variable(s)	Spatial Resolution	Temporal Resolution	Use	Reference
StageIV	Precipitation	4 km	hourly	Forcing	Baldwin and Mitchell (1998) Du (2011)
NLDAS-2 Forcing File A	Atmospheric	0.125°	hourly	Forcing/Data Assimilation	Mitchell et al. (2004)
NLDAS-2 Mosaic	Vegetation Fraction/ Albedo	0.125°	hourly	Forcing/Data Assimilation	Xia et al. (2012)
MODIS MOD15A2H	LAI/FPAR	500 m	8 day	Forcing/Data Assimilation	Myneni et al. (2015)
MODIS MOD12Q1	Land Cover	500 m	yearly	Forcing	Friedl and Sulla-Menashe (2015)
STATSGO	Soil Texture and Porosity	30 arcsec	fixed	forcing	Miller and White (1998)
AmeriFlux	GPP, latent heat, SM	point	30 min.	Validation	Baldocchi et al. (2001)
MODIS MOD17A2H	GPP	500 m	8 day	Validation	Running et al. (2015)
Noah-LSM	SM	0.125°	hourly	Validation	Xia et al. (2012)
SMERGE	SM	0.125°	hourly	Validation	Tobin et al. (2019)

2.2 Forcing Data Sets

2.2.1 Meteorological

The 1-D DCHM (-V and -PV) spatial and temporal resolution is set to the scale of the available precipitation forcing data. For this study, we use the native resolution of the Stage-IV precipitation forcing from the National Oceanic and Atmospheric Administration (NOAA) National Centers for Environmental Prediction (NCEP) (Baldwin and Mitchell, 1998; Du, 2011). The

https://doi.org/10.5194/hess-2023-146
Preprint. Discussion started: 11 July 2023


Hydrology and Earth System Sciences
Discussions

Stage-IV dataset has 4 km spatial resolution and 1 h temporal resolution and is available beginning from 2002. Atmospheric forcing data used in the DCHM are from the North America Land Data Assimilation System Phase 2 (NLDAS-2) Forcing File A. NLDAS-2 is a combination of observational and reanalysis data sets (Mitchell et al., 2004) intended for use in land surface models like the DCHM. The data are available at 0.125 degree spatial resolution and interpolated to the 4 km Stage-IV grid. No temporal interpolation was necessary.

2.2.2 Land Cover

The land surface albedo and fraction of vegetation cover come from NLDAS-2 Mosaic Land Surface Model L4 dataset (Xia et al., 2012; Mitchell et al., 2004). NASA's Moderate Resolution Imaging Spectroradiometer (MODIS) MCD12Q1 remotely sensed satellite data product is used to inform the model of land cover classification. In particular, we use the University of Maryland classification scheme (Sulla-Menashe and Friedl, 2018). Within the model, the classification is updated yearly. The native spatial resolution of this data set is 500 m and we interpolated to the 4 km size for model implementation using a most frequent approach.

2.2.3 Soil Texture and Porosity

Soil texture and porosity data was acquired from Soil Information for Environmental Modeling and Ecosystem Management CONUS-Soil (Miller and White, 1998). The CONUS-Soil spatial resolution is 1 km with 11 layers. We upscaled the raw soil texture and porosity data to the 4-km Stage-IV grid. For each pixel, we approximate soil porosity by averaging the top eight layers (100 cm) and we represent texture using the most frequent texture. By averaging over the top 100 cm, we avoid averaging layers interpolated as bedrock, and thus near zero porosity.

2.2.4 Vegetation

MODIS LAI and FPAR data were downloaded for all of CONUS at the native 500-m spatial and 8 day temporal resolution. Before scaling to the DCHM grid and time scale, the data for each pixel were smoothed using a Savitsky-Golay (Savitzky and Golay, 1964) algorithm following Chen et al. (2004) in order to preserve seasonality and reduce noise associated with cloud cover and other atmospheric effects (Cihlar et al., 1997; Tanré et al., 1997). We use the m=6 scaling window and d=4 degree of the interpolating polynomial as in Chen et al. (2004) and Lowman and Barros (2016). After the smoothing filter is applied, the data is up-scaled from 500 m to 4 km resolution and linearly interpolated to a 1 h temporal resolution.

2.3 Validation Data Sets

We use the flash drought of 2012 to compare model results to multiple ground and remotely sensed observations. Modeled soil moisture (SM) fluxes are compared to SoilMERGE (SMERGE), a 0.125 degree root-zone (0-40 cm) SM product obtained from 'merging' NLDAS-2 outputs with European Space Agency Climate Change Initiative surface satellite data which can predict vegetation health anomalies (Tobin et al., 2019). We also validate SM estimates against simulated SM from Noah land-

https://doi.org/10.5194/hess-2023-146
Preprint. Discussion started: 11 July 2023

Hydrology and Earth System Sciences
Discussions
Open Access
EGU

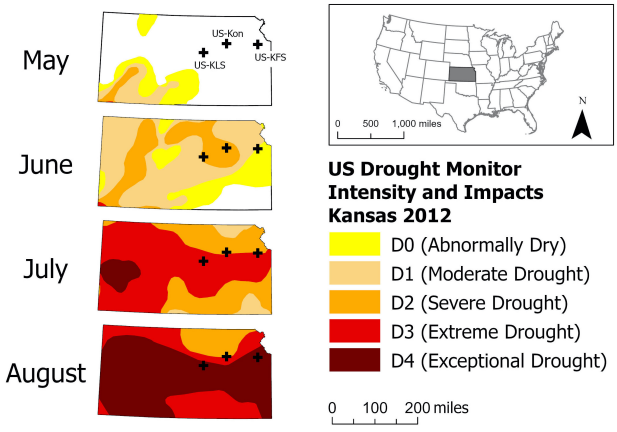

Figure 2. Maps of the U.S. Drought Monitor with the three AmeriFlux tower sites (US-KFS, US-KLS, and US-Kon) showing the evolution of the U.S. flash drought of 2012.

surface model (LSM) for all three root zones used in DCHM. Noah-LSM is a physically based model forced with NLDAS-2 Forcing File A (Xia et al., 2012)). When AmeriFlux SM data is available, we compare with modeled soil moisture from the top layer since most AmeriFlux SM sensors are in the top few centimeters of soil. Computed outputs of GPP are compared to MODIS (MOD17A2H) GPP product and AmeriFlux eddy covariance outputs of GPP. We computed ET from AmeriFlux eddy covariance flux tower values by dividing latent heat flux by the latent heat of vaporization of water and use the results to validate model outputs of ET.

2.4 Model Site Locations

This study employs eddy covariance data from three AmeriFlux sites in Kansas (US-KFS, US-KLS, US-Kon, Figure 2 and Table 2). Each site was chosen because of the availability of GPP and latent heat (converted to ET) data during the flash drought year of 2012 and at least one wet year after 2012. Static characteristics of PFT, soil texture and porosity, and geographic information for the study sites are shown in Table 2. According to the MODIS land cover classification product (MCD12Q1), each site had a unique vegetation cover type (savanna, grassland, cropland, Table 2). The PFT is a result of interpolating MODIS MCD12Q1 Land Cover Type 2 to the 4-km grid and does not necessarily align with the land cover from AmeriFlux. The soil texture and porosity are interpolated CONUS-Soil (Miller and White, 1998) values.

2.5 Model Description

We employ two 1-D versions of the DCHM coupled land-surface hydrology model that accounts for mass (water) and energy transfers between three soil layers, the surface, and the atmosphere (Devonec and Barros, 2002)) applied on a 4-km grid. The 4-km grid was chosen since it is the native spatial resolution of the Stage-IV data, as precipitation is the main source of uncertainty when modeling drought (Trenberth et al., 2014). The soil depths we use best match the USDA Kansas soil profile

https://doi.org/10.5194/hess-2023-146
Preprint. Discussion started: 11 July 2023

Hydrology and Earth System Sciences
Discussions

Table 2. AmeriFlux study sites contained within StageIV pixels.

Site	Latitude	Longitude	PFT	Texture	Porosity	Reference	Annual Precipitation [mm]		
							AmeriFlux mean	StageIV 2012	StageIV 2019
US-KFS	39.0561	-95.1907	SAV	silty clay loam	0.4225	Brunsell (2020a)	1012	597	1373
US-KLS	38.7754	-97.5684	CRO	silt loam	0.4812	Brunsell (2021)	812	558	1425
US-Kon	39.0824	-96.5603	GRA	silty clay loam	0.4588	Brunsell (2020b)	867	490	1346

Plant functional type (PFT), soil texture, and porosity determined after interpolation to the StageIV grid. Abbreviations: SAV = Savanna, CRO = Cropland, GRA = grassland.

(Soil Survey Staff). We maintain 8 cm for the top soil layer for model stability, but use 35 in. (approx 89 cm) for root zone depth and 72 in (89-183 cm) for the impermeable layer. This yields the three soil layers: top (0-8 cm), middle (8-89 cm), and bottom (89-183 cm). Each PFT has its own root distribution function dictating root water uptake through the three layers (Lowman and Barros, 2016; Zeng, 2001; Lai and Katul, 2000; Clausnitzer and Hopmans, 1994).

The water balance includes subroutines for evaporation from the different land surfaces (bare soil, vegetation), ponding and groundwater runoff, snow hydrology, and root water uptake while energy balance routines solve for net radiative fluxes, sensible and latent heat transfers, and ground heat fluxes (Lowman and Barros, 2018, 2016; Tao and Barros, 2014, 2013; Yildiz and Barros, 2007, 2005; Garcia-Quijano and Barros, 2005; Devonec and Barros, 2002; Barros, 1995). The water and energy balances are linked through parameterized routines for photosynthesis following the Farquhar model (Lowman and Barros, 2016; Garcia-Quijano and Barros, 2005; Farquhar and Caemmerer, 1982; Farquhar et al., 1980).

The main difference between the DCHM-V and DCHM-PV is that the DCHM-V has vegetative phenology forced with updates from MODIS MOD15A2H FPAR and LAI products and the DCHM-PV implements a subroutine for predicting phenology (DCBP). The DCHM-PV is run using an ensemble of parameters (Table 4) generated using an Ensemble Kalman Filter (EnKF) from outputs from the DCHM-V following Lowman and Barros (2018) with a separate simulation for each ensemble member.

Establishing differences in the outputs from DCHM-V and -PV illuminate changes in plant behavior. MODIS is a passive sensor and observes only the red (648 nm) and near-infrared (NIR, 858 nm) spectral bands to estimate values of LAI (Myneni et al., 2015). The DCBP model predicts plant life stage based on climatological properties of water availability, air temperature, and evaporative demand (Lowman and Barros, 2018). We updated FPAR and LAI instead of forcing them with MODIS observations to evaluate impacts on estimates of ET and GPP (Lowman and Barros, 2018; Kim et al., 2015; Caldararu et al., 2014). Predicting phenological state variables also provides updates on daily time scales rather than through interpolation from the 8 day measurements of MODIS. We compare model outputs for a wet year and a dry year to illuminate the vegetation responses to flash drought.

https://doi.org/10.5194/hess-2023-146
Preprint. Discussion started: 11 July 2023


Hydrology and Earth System Sciences
Discussions

The data assimilation procedure within the predictive phenology model jointly estimates the current phenological state (FPAR, LAI) along with eleven parameters (Table 4) required to calculate the next phenological state (Lowman and Barros, 2018). This method was first introduced by Moradkhani et al. (2005) as a way of simultaneously predicting states and parameters in hydrology models, and it was later implemented by Stöckli et al. (2008) specifically for assimilating remotely sensed data in phenological models. Lowman and Barros (2018)) added additional soil water parameters to the data assimilation system to improve phenological state predictions. Using outputs from the DCHM-V and updating phenological states from MODIS FPAR and LAI in the DCBP, we generate ensembles of phenology parameters representing different precipitation regimes (above average, below average, and mixed conditions). We run Monte-Carlo simulations of the DCHM-PV with N=2000 ensembles of the DCBP model parameters. Ensembles were generated using the final mean and standard deviations of the parameters from each inference period.

2.6 Model Simulations

We begin by running the DCHM-V from 2002-2019 (spinning-up 2002 three times to allow for model stabilization, Lowman and Barros (2016, 2018)) for all three sites. Using the DCHM-V outputs from 2003-2005 along with the DCBP, we generate ensembles (N=2000) of phenology model parameters for three meteorological scenarios for each site (Table 3) yielding a total of twelve simulations (one DCHM-V and three DCHM-PV for each of the three sites). Each of the nine phenology ensembles consist of 2000 sets of parameters so each of the nine DCHM-PV simulations consist of 2000 Monte Carlo experiments. We chose the 2003-2005 period because it allows us to establish ensembles of phenology parameters associated with dry, wet, and mixed condition periods. The parameters used in the DCHM-PV simulations are from the one-year periods of 2003 (DRY) and 2005 (WET), and from the three-year period 2003-2005 (3YR). The chosen assimilation period is prior to the case studies described in Section 2.7, thereby preventing the use of over fit model parameters when investigating the behavior of the DCHM-PV results. The three sets of phenology parameters for each site allows us to investigate vegetation-atmosphere feedbacks through different causal lenses by generating phenology model parameters in several climate scenarios. Furthermore, this type of simulation permits us to investigate if meteorological conditions alter plant behavior (become more isohydric or anisohydric), rather than investigating if vegetation behavior affects the development of flash drought. Broadly speaking, vegetation model parameters trained on dry conditions will represent isohydric vegetation and vice versa for vegetation trained on

Table 3. Summary of precipitation conditions during assimilation periods.

		StageIV Annual Precipitation Accumulation [mm]		
Year(s)	Abbreviations	US-KFS	US-KLS	US-Kon
2003-2005	3YR	1066	770	847
2003	DRY	804	756	670
2005	WET	1242	806	956

https://doi.org/10.5194/hess-2023-146
Preprint. Discussion started: 11 July 2023

Hydrology and Earth System Sciences
Discussions

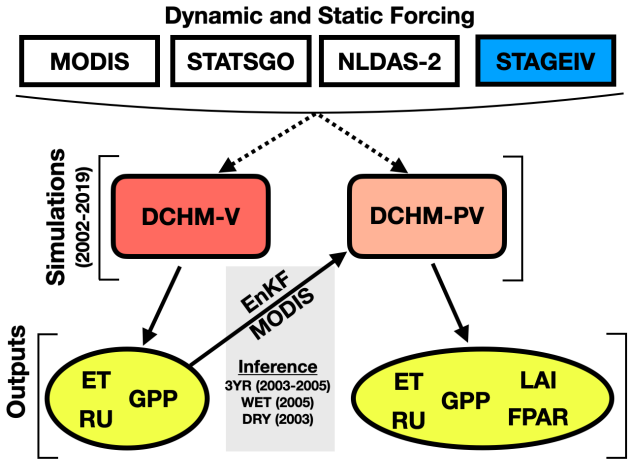

Figure 3. Schematic of modeling workflow. Spatial and temporal resolutions of all forcing data match Stage IV precipitation (4 km and 1 h) and dictate DCHM scales. Land cover, soil properties, and atmospheric forcing inputs come from MODIS, STATSGO, and NLDAS-2, respectively. Simulations are run from 2002-2019. Three ensembles of parameters for the predictive phenology routine in the DCHM-PV are determined using an ensemble Kalman filter (EnKF) with DCHM-V outputs, MODIS MOD15A2H FPAR/LAI, and concurrent meteorological conditions from 2003 (DRY), 2005 (WET), and 2003-2005 (3YR). DCHM-V outputs of interest include evapotranspiration (ET), Root water uptake (RU), and gross primary productivity (GPP). Additional DCHM-PV outputs include predicted fraction of photosynthetically active radiation (FPAR) and leaf area index (LAI).

wet conditions because vegetation adapted to minimal rainfall is more conservative in its water use (Lowman and Barros, 2018; Sade et al., 2012). By using the three different data assimilation periods, we are able to capture the sensitivity of phenology model parameters to the meteorological conditions.

2.7 Study Period and Outputs

We run the DCHM-V and DCHM-PV for 2002-2019. We are able to generate phenology parameters using a subset of this time frame (2003-2005), allowing us to investigate land-atmosphere interactions outside of the parameter inference period. We highlight results from the three AmeriFlux sites for 2012 (flash drought) and 2019 (above average precipitation) to draw conclusions about plant responses during flash drought. We are also able to compute yearly totals of GPP and ET from 2006-2019 to assess interannual variability of outputs from DCHM-V and DCHM-PV. Transpiration is calculated from total root water uptake through the three soil layers to partition ET into evaporation and transpiration (Lowman and Barros, 2018; Lai and Katul, 2000). Water use efficiency is represented as the ratio of GPP and ET (WUE = GPP/ET, Beer et al. (2009)). We highlight differences between the DCHM-V and DCHM-PV model simulations and compare outputs to remotely sensed and in situ observations where available.

https://doi.org/10.5194/hess-2023-146
Preprint. Discussion started: 11 July 2023

Hydrology and Earth System Sciences
Discussions

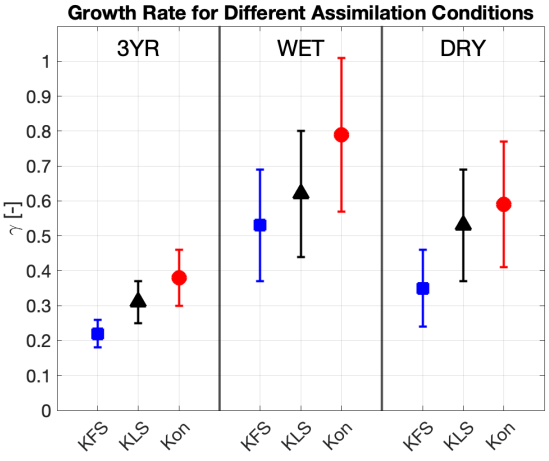

Figure 4. Growth rate parameters with one standard deviation for each site for all three data assimilation periods: 3YR (2003-2005), WET (2005), DRY (2003).

3 Results

We first present phenology model parameters as estimated from the data assimilation procedure. Then, we show DCHM-V (forced phenology) and DCHM-PV (predictive phenology) results.

3.1 Phenology

3.1.1 Phenology Model Parameters

The growth rate parameter, γ, dictates how much phenological state (i.e. FPAR and LAI) can change in a given time step (Lowman and Barros, 2018; Stöckli et al., 2008). Lower uncertainty in the growth rate parameter establishes the 3YR assimilation period, with a mixture of wet and dry years, as the preferred choice for running the DCHM-PV (Figure 4) and is in agreement with Lowman and Barros (2018). This lower uncertainty propagates through the DCBP in the DCHM-PV, reducing uncertainty in the predictions of FPAR and LAI (Figures 5 and 6). The values of gamma vary by site, and therefore plant function type (PFT). The smaller magnitudes of the growth parameters indicates that vegetation is less likely to make abrupt changes and exhibit more resilience when faced with extreme dry down. Other parameter estimation outputs used to generate ensembles from the 3YR assimilation period can be found in Table 4.

3.1.2 FPAR

Results indicate slower senescence and reduced variance using the 3YR assimilation parameters during late June and early July 2012 across all three sites. A decrease in FPAR can be seen in late June 2012 across all simulations (Figure 5). This aligns with the known period of flash drought that occurred across Kansas (Lisonbee et al., 2021). For each site, the simulated FPAR

https://doi.org/10.5194/hess-2023-146
Preprint. Discussion started: 11 July 2023

Hydrology and Earth System Sciences
Discussions
Open Access
EGU

Table 4. Phenology model parameters from 3YR assimilation period.

			Mean parameter estimates ± one standard deviation		
Parameter	Description	Units	US-KFS	US-KLS	US-Kon
$T_{min_{min}}$	Minimum value of daily minimum temperature	°C	-5.5 ± 3.1	0.1 ± 2.4	-2.3 ± 3.2
$T_{min_{max}}$	Maximum value of daily minimum temperature	°C	14.0 ± 1.8	16.5 ± 1.8	15.8 ± 2.0
Pht_{min}	Minimum daily exposure to sunlight	h	10.0 ± 0.4	9.8 ± 0.6	10.7 ± 0.6
Pht_{max}	Maximum daily exposure to sunlight	h	14.3 ± 0.3	14.2 ± 0.4	14.3 ± 0.4
$VPD_{avg_{min}}$	Minimum daily average vapor pressure deficit	mb	17.1 ± 1.3	16.6 ± 1.4	16.9 ± 1.4
$VPD_{avg_{max}}$	Maximum daily average vapor pressure deficit	mb	58.7 ± 2.3	55.8 ± 2.2	55.6 ± 2.3
$\psi_{soil,avg_{min}}$	Minimum daily average soil water potential	J kg^{-1}	-42.1 ± 5.6	-37.2 ± 5.8	16.9 ± 5.5
$\psi_{soil,avg_{max}}$	Maximum daily average soil water potential	J kg^{-1}	-7.4 ± 1.3	-7.0 ± 1.4	-6.9 ± 1.4
$FPAR_{min}$	Minimum fraction of photosynthetically active radiation	-	0.31 ± 0.01	0.35 ± 0.01	0.31 ± 0.01
LAI_{max}	Maximum leaf area index	m^{2}m^{-2}	6.36 ± 0.15	6.51 ± 0.17	6.65 ± 0.18
γ	growth rate	day^{-1}	0.22 ± 0.04	0.31 ± 0.06	0.38 ± 0.08

from the 3YR assimilation phenology parameters shows a less dramatic response in the decrease in FPAR when compared to the DCHM-PV simulations using the WET and DRY parameters. The predicted values of FPAR at US-KFS and US-KLS are slightly higher than the MODIS values during the 2012 growing season. The predicted values of FPAR match well against MODIS for the US-Kon site, especially during the decline in late June through July. During the flash drought period, there is a notable decrease in variance, or uncertainty, across the Monte Carlo simulations.

For US-KFS across the three simulations, the simulation using the WET parameters achieves a higher FPAR during the flash drought and holds its peak throughout the month of May, with declines beginning in June and bottoming in early July before rising again in the latter part of the growing season. The decrease in FPAR for the WET parameters is from 0.77 to 0.41 while reductions from the time of peak FPAR to early July in the simulations using DRY and 3YR parameters are from 0.73 to 0.47 and 0.76 to 0.53, respectively.

Results from an above average precipitation year (2019) show a steady increase, a longer peak season, and a decrease in line with fall senescence across all simulations, though WET and DRY parameters at US-KLS both lead to a phenological response in July 2019, likely due to the below average July precipitation. Overall, the simulations tend to follow the same patterns as MODIS throughout the growing season, irrespective of choice of parameters. Similar to the 2012 results, simulations using phenology parameters from the 3YR assimilation period showed slower late-season declines in FPAR than the simulations using parameters derived from the WET or DRY assimilation periods. This behavior can be seen from the 3YR parameter simulations for US-KLS and US-Kon which show higher FPAR through July. At these sites, the dip in July FPAR using the

https://doi.org/10.5194/hess-2023-146
Preprint. Discussion started: 11 July 2023

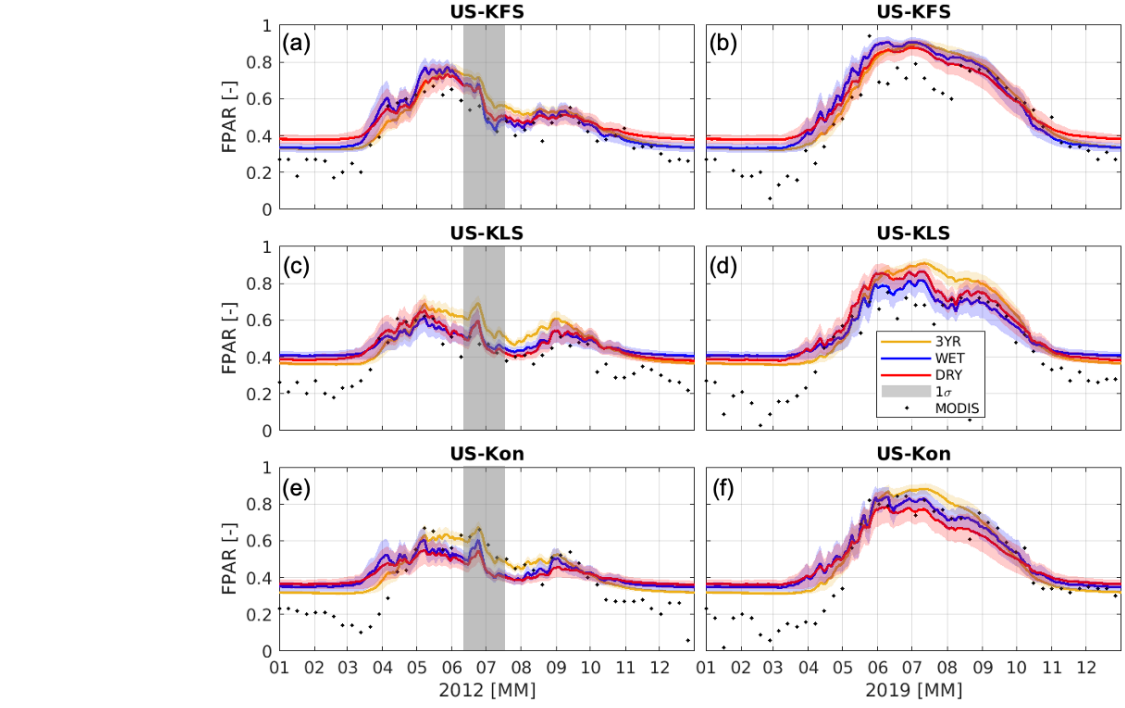

Figure 5. Time series of fraction of photosynthetically active radiation (FPAR) predicted from DCHM-PV for the flash drought year (2012) and an above average precipitation year (2019) for the three AmeriFlux study sites (US-KFS, US-KLS, US-Kon). The different colors represent the usage of parameters from the different data assimilation periods (yellow - 3YR (2003-2005), blue - WET (2005), red - DRY (2003), with corresponding shaded regions representing one standard deviation of model outputs from the 2000 ensemble simulations. 8 day MODIS MOD15A2H FPAR is indicated with black markers. The gray shaded region highlights the June to July decrease in FPAR during the 2012 flash drought.

WET and DRY parameters is likely due to the susceptibility of abrupt changes in response to minimal July rainfall. At US-KFS, the three different simulations vary little from one another which could be due to the savanna representation at US-KFS and its resiliency to the minimal July precipitation during 2019. Despite the minimal July rainfall, phenological stages were generally resilient due to the abundance of soil water from early precipitation.

3.1.3 LAI

Predicted values of LAI are similar to MODIS LAI, with relative differences between DCHM-PV and MODIS similar to the FPAR results (Figure 6). During the flash drought year of 2012, a steep decline in modeled LAI can be seen in late June and early July across the three sites. The LAI experienced declines of almost 1 m^2m^{-2} in just a few days. DCHM-PV model outputs of LAI during 2019 match MODIS but are 1-2 m^2m^{-2} higher during June, July, and early August at US-KFS and US-KLS, and slightly lower than MODIS at US-Kon. Simulated LAI vary slightly across the three sites. For US-KFS, simulations

https://doi.org/10.5194/hess-2023-146
Preprint. Discussion started: 11 July 2023

Hydrology and Earth System Sciences
Discussions

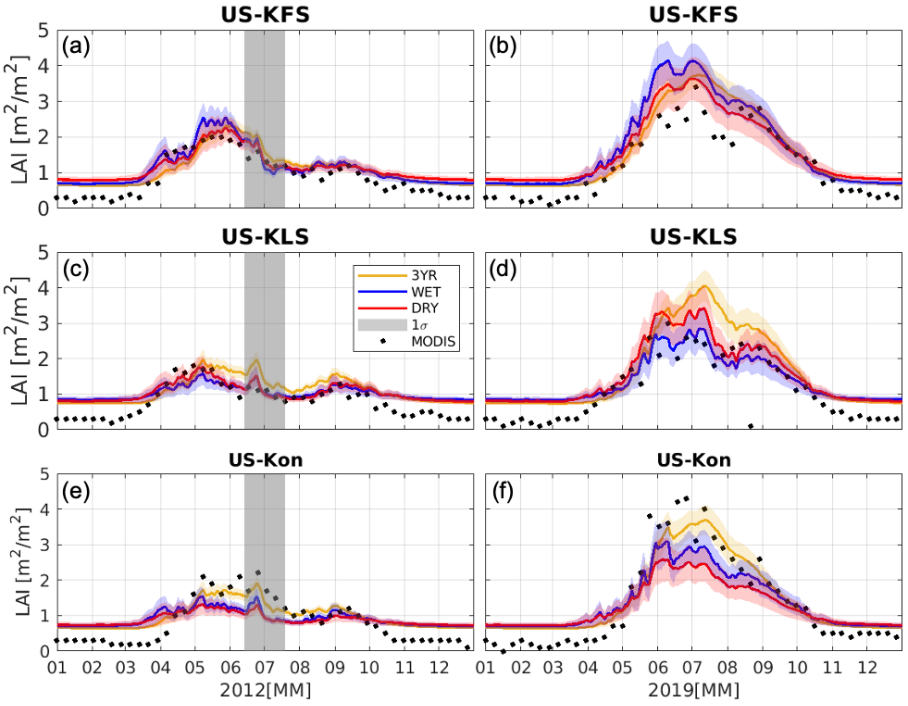

Figure 6. Time series plots of leaf area index (LAI) predicted from DCHM-PV for the flash drought year (2012) and an above average precipitation year (2019) for the three AmeriFlux study sites (US-KFS, US-KLS, US-Kon). The different colors represent the usage of parameters from the different data assimilation periods (yellow - 3YR (2003-2005), blue - WET (2005), red - DRY (2003)), with corresponding shaded regions representing one standard deviation of model outputs from the 2000 ensemble simulations. 8 day MODIS MOD15A2H LAI is indicated with black markers. The gray shaded region highlights the June to July decrease in FPAR during the 2012 flash drought.

using the WET year parameters achieve higher values in LAI than the other two simulations (Figure 6 a,b). For US-KLS, and US-Kon, the growing season LAI has the highest peaks in the simulations using the 3YR parameters (Figure 6 c,d). With more rainfall in May and June 2019, the simulations using the WET parameters show lower LAI than the simulations using the DRY parameters.

The most consistent similarities across the phenology results is that the simulations using the 3YR parameters generally show a slower decline in LAI in both a flash drought year and a wet year for all sites. Another similarity across these figures is that simulations using WET and DRY parameters align with one another more than they match the simulations using 3YR parameters. This result is commensurate with the values of the means and variances of the growth rate parameters resulting from the different assimilation periods.

Differences in the growth rate parameter can also be seen in LAI outputs from the simulations of the DCHM-PV (6). During the 2012 flash drought, simulations using the 3YR assimilation period show LAI staying high for a longer period of time, and the decrease develops slower than the other two simulations. This feature is also apparent in the 2019 plots for US-KLS and

https://doi.org/10.5194/hess-2023-146
Preprint. Discussion started: 11 July 2023

Hydrology and Earth System Sciences
Discussions

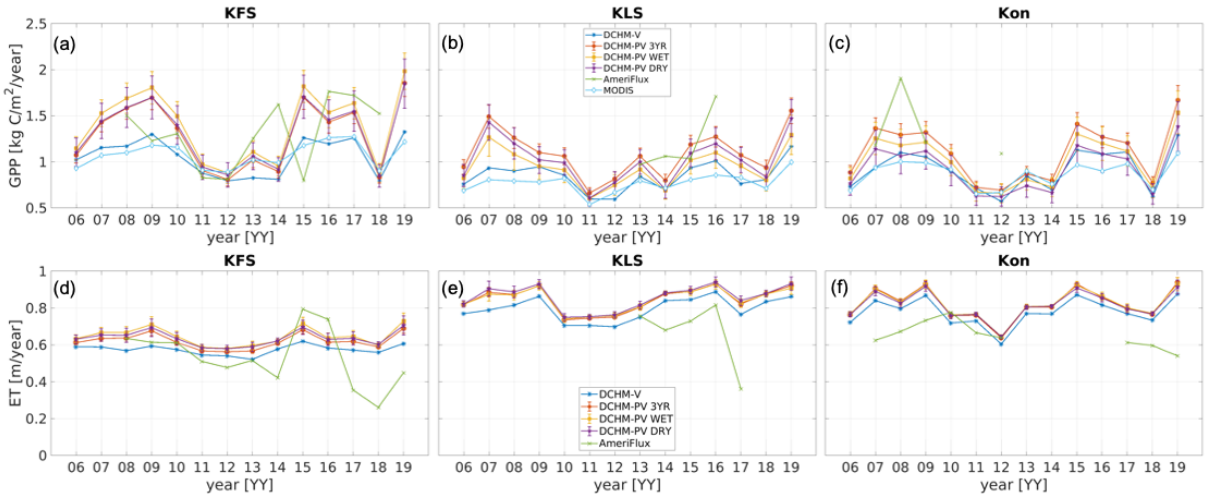

Figure 7. Time series of yearly totals of GPP and ET for 2006-2019 at US-KFS, US-KLS, and US-Kon from DCHM-V, three DCHM-PV, AmeriFlux, and MODIS (GPP only). Yearly totals from the 2000 DCHM-PV Monte Carlo simulations are shown as ensemble means and one standard deviation indicated by error bars. Estimates of ET from AmeriFlux were generated by dividing measurements of latent heat by the coefficient of vaporization and were eliminated from the analysis if more than 20% of the yearly data was missing.

US-Kon. In the 2019 plots, simulations continue to show growth through June, with peaks occurring in the middle of July, while the LAI in plots of the WET and DRY simulations seem to flatten their growth from the beginning of June to mid-July.

3.2 Vegetation Responses

3.2.1 GPP

Yearly totals (2006-2019) of GPP are shown in Figure 7 a-c for each site. The points used in the yearly time series represent the ensemble means from DCHM-PV and yearly totals from DCHM-V, MODIS, and AmeriFlux tower records. The DCHM-PV yearly totals of GPP at US-KFS and US-Kon are similar to totals estimated for the same sites in another study which updated LAI and vegetation cover dynamically using Noah-MP (Hosseini et al., 2022). Ameriflux tower yearly totals were discarded from the analysis if more than 20% of the data were missing for the year. The error bars on the DCHM-PV plots show one standard deviation from the mean for the 2000 ensemble members. Carbon uptake during water stress years is about 1 kgCm^{-2} less than during years experiencing above average precipitation. The DCHM-V, which uses MODIS to update vegetation state indices (FPAR and LAI), compares well in magnitude to MODIS GPP yearly assimilation rates. In periods where there is no water stress (e.g., 2019), the DCHM-PV predicts more carbon assimilation than DCHM-V and MODIS. All simulations show major declines in net carbon assimilation during the 2012 flash drought.

We highlight the seasonal variation of GPP at US-KFS (Figures 8, A11, A12) for simulations from the DCHM-V and -PV (3YR) with observations from MODIS and AmeriFlux for the flash drought year (2012) and an above average precipitation year

https://doi.org/10.5194/hess-2023-146
Preprint. Discussion started: 11 July 2023

Hydrology and Earth System Sciences
Discussions
Open Access
EGU

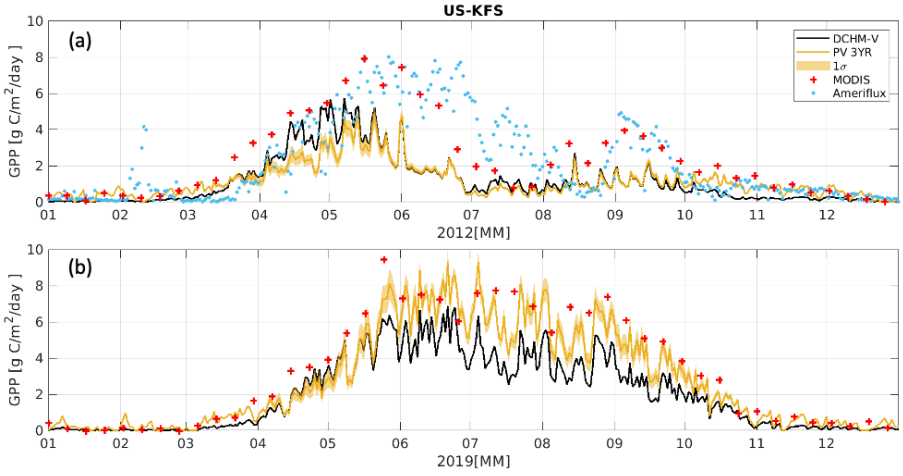

Figure 8. Time series from the DCHM-V, DCHM-PV three year assimilation period, 8 day MODIS, and daily AmeriFlux totals of GPP at US-KFS for (a) 2012, flash drought year and (b) 2019, an above average precipitation year.

(2019). We observe that during the growing season of 2019, the simulations all predict GPP on par with MODIS, but during the flash drought of 2012, the DCHM simulations (both -V and -PV) respond to the dry down earlier than either MODIS or the tower. In particular, in late June to early July 2012, carbon uptake decreases from 5.0 to 0.7 $gCm^{-2}day^{-1}$. From these plots, we can also notice that uncertainties from the ensemble runs are largest during the green up period, but are generally smaller in the flash drought year than in the above average precipitation year.

3.3 ET

Yearly ET totals for 2012 are approximately 0.1 m yr^{-1} less than maximum at US-KFS (Figure 7 d) and 0.2 m yr^{-1} at the other sites (Figure 7 e,f). DCHM-PV simulations (using WET, DRY, and 3YR) tend to estimate higher ET than the DCHM-V and lower ET than that observed by AmeriFlux (Figure 9 with other sites in appendix, Figures A13 and A14). The Monte Carlo simulations indicate uncertainty is smaller during the flash drought (Figure 9). Overall uncertainty in ET increases during the green up period at the beginning of the growing season (April). The differences in simulated ET among the different assimilation strategies are most apparent during the early months of the growing season (April - May) with the WET assimilation showing highest rates of ET. During the 2012 flash drought from June through August, outputs of ET were similar across simulations with different phenology model parameters. Peaks in ET occur after precipitation events with extended declines and troughs between rain events. The amount of troughs and the corresponding ET rates are indicative of slowed vegetation activity in response to the water stress.

When ET was partitioned into evaporation and transpiration during the flash drought, transpiration gradually declined. Resulting large fluctuations in total ET are a result of evaporation in response to precipitation (Figure 10a). This suggests water evaporated before it had a chance to infiltrate the soils and be absorbed by the vegetation root systems. Since we compute

https://doi.org/10.5194/hess-2023-146
Preprint. Discussion started: 11 July 2023

Hydrology and Earth System Sciences
Discussions
Open Access
EGU

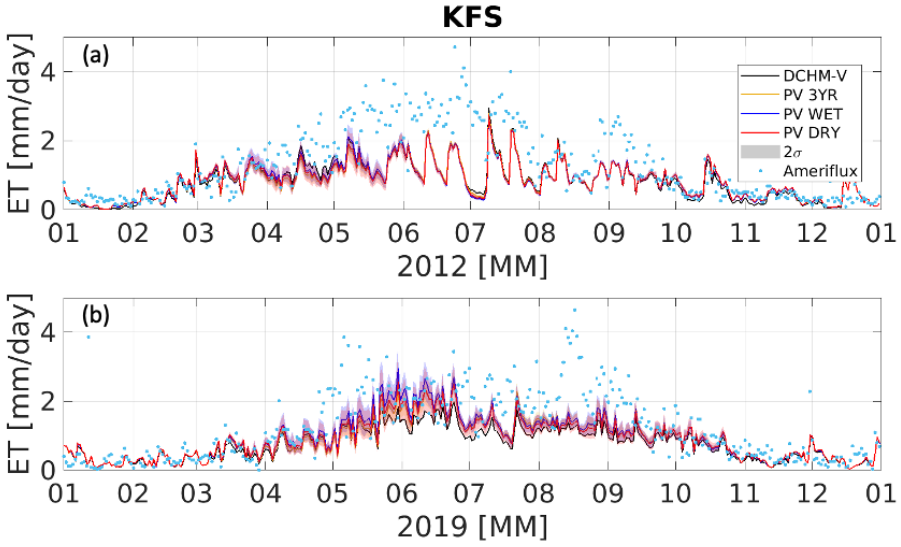

Figure 9. Time series of ET at US-KFS for (a) 2012, flash drought year and (b) 2019, wet year from DCHM-V and three different DCHM-PV simulations. Two standard deviations are shown for DCHM-PV simulations. AmeriFlux ET is showing with the blue markers.

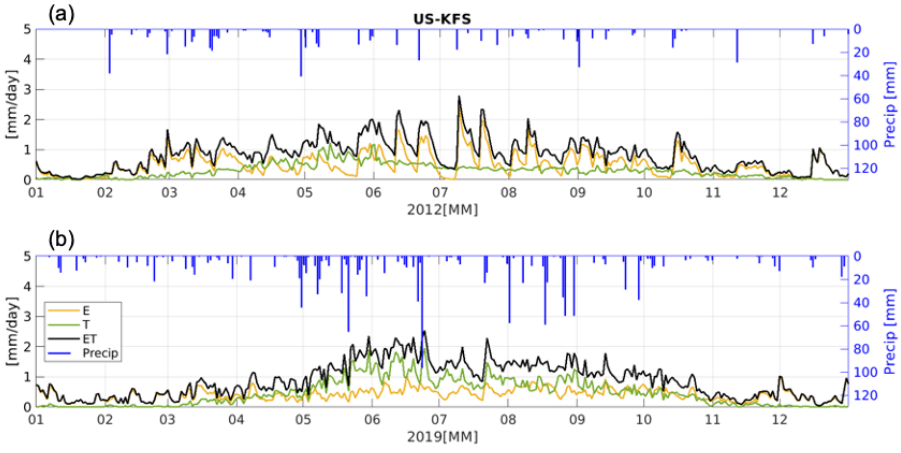

Figure 10. Ensemble means of simulated evapotranspiration partitioned into evaporation (E) and transpiration (T) for US-KFS in (a) 2012, flash drought and (b) 2019, wet year. Transpiration totals are in DCHM from total root uptake across the three soil layers. The top axis is daily StageIV precipitation totals.

transpiration from root water uptake through the three soil layers, the observation that transpiration decreases but still maintains a small rate through the flash drought is indicative of vegetation extracting water from the deeper soil layers as it undergoes stress. ET never completely shuts down because there is always a small rate of transpiration. Evaporation reaches zero during early July 2012, which is the peak of the flash drought period.

https://doi.org/10.5194/hess-2023-146
Preprint. Discussion started: 11 July 2023


Hydrology and Earth System Sciences
Discussions

In contrast to 2012, during 2019 there was ample rainfall and water available for plant use throughout the growing season. Despite minimal rainfall in early July 2019, we observe DCHM-PV (3YR) model predictions of decreased ET in response to the lower rainfall, but transpiration rates were still higher than evaporation rates throughout the growing season (Figure 10b). During the growing season, transpiration rates usually comprise more than 50% of total ET at US-KFS, a finding that aligns with results from Hosseini et al. (2022) who used the Noah-MP Land Surface Model which also computes transpiration from root water uptake (Li et al., 2021). However, during the flash drought year of 2012, transpiration rates fell below 35% of overall ET at US-KFS (Figure 12a). Partitioned transpiration decreases approximately 40% from May to June at US-KLS (Figure 12b), and 20% at US-Kon (Figure 12c). The rapid decline in transpiration rates can be attributed to the slowing of root uptake due to the lack of available water. The transpiration rates follow changes in GPP during the flash drought of 2012 (Figure A17a). However, ET decreases at US-KFS during July 2019 while experiencing a brief period of low rainfall (Figure 10b), yet is able to maintain rates of GPP during this period due to the amount of available water in soils from the excessive precipitation during May and June (Figures A2, A4, A6).

4 Discussion

4.1 Vegetation Responses to Flash Drought

Vegetation responses to water stress can be seen through fluctuations in GPP (Zhang and Yuan, 2020; Jin et al., 2019) and ET (Chen et al., 2019). Decreases in GPP occur when plants close their stomata. With the stomata closed, plants will not undergo normal gas exchange through photosynthesis and decrease their transpiration rates. Transpiration is only one part of ET, so we must be careful not to directly link fluctuations in GPP with fluctuations in ET. Evaporation can still be high when there is little to no transpiration, but GPP tend to follow the same trajectories as transpiration (Beer et al., 2009). The DCHM accounts for evaporation of water intercepted by the canopy, water that has ponded on the ground, and water in the top soil layer. At the onset of flash drought there is an increase in evaporative demand for water which leads to a temporary increase in surface evaporation (Lowman et al., in press; Otkin et al., 2018) until the soil and canopy reservoirs no longer contain enough water to evaporate. Then evaporation shuts down. With small rates of transpiration still occurring, small rates of GPP are maintained (i.e. carbon uptake drastically slows, but it does not stop, Figure A17a) which affects plant WUE (Figure 11a). These results align with our initial hypotheses (H1, H2). However, we did find that even during the peak flash drought, plants were still pulling small amounts of water from deep soil layers, allowing for transpiration and carbon exchanges, preventing plants from complete shut down.

We compare simulated and observed data to determine how vegetation regulates its water use, either pulling water from deeper or shutting down transpiration. We compare the timing of fluctuations in GPP and ET by combining previous plots together on the same axes (Figure A17). During the flash drought of 2012 (mid May - early July), we estimated steady declines in rates of GPP with bursts in ET corresponding to rain recharge events. This implies evaporation may be the main contributor to total ET during the flash drought since GPP is decreasing (Figures 8a and A17a). The decreases in GPP due to flash drought during June and July 2012 are consistent in terms of magnitude withdecreases found in recent studies (Yao et al., 2022; Poonia

https://doi.org/10.5194/hess-2023-146
Preprint. Discussion started: 11 July 2023

Hydrology and Earth System Sciences
Discussions

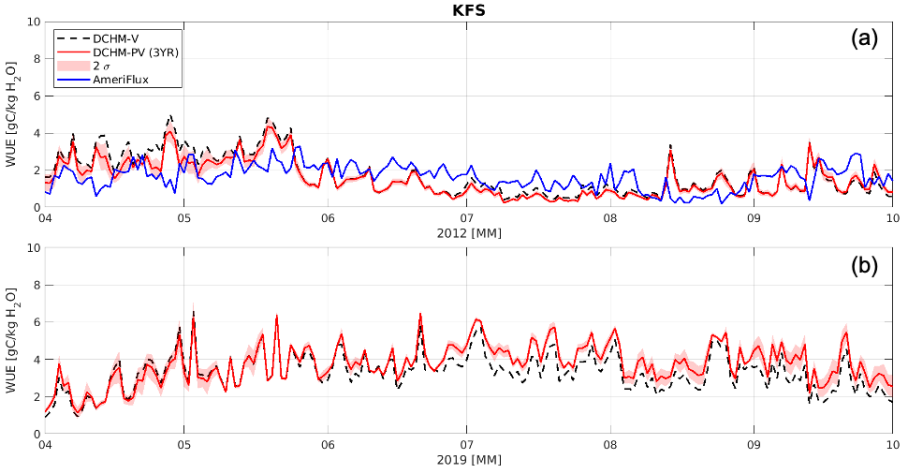

Figure 11. Computed growing season water use efficiency (WUE=GPP/ET) from DCHM-V, DCHM-PV (3YR), and AmeriFlux for (a) 2012, flash drought and (b) 2019, wet year at US-KFS. AmeriFlux WUE computed by converting latent heat into ET by dividing by the coefficient of vaporization.

et al., 2022; Zhang et al., 2020). These decreases are attributed to changes in transpiration during flash drought (Figure 10a). We also find that when plants are transpiring more, they are more efficient in their water use (Figure 12).

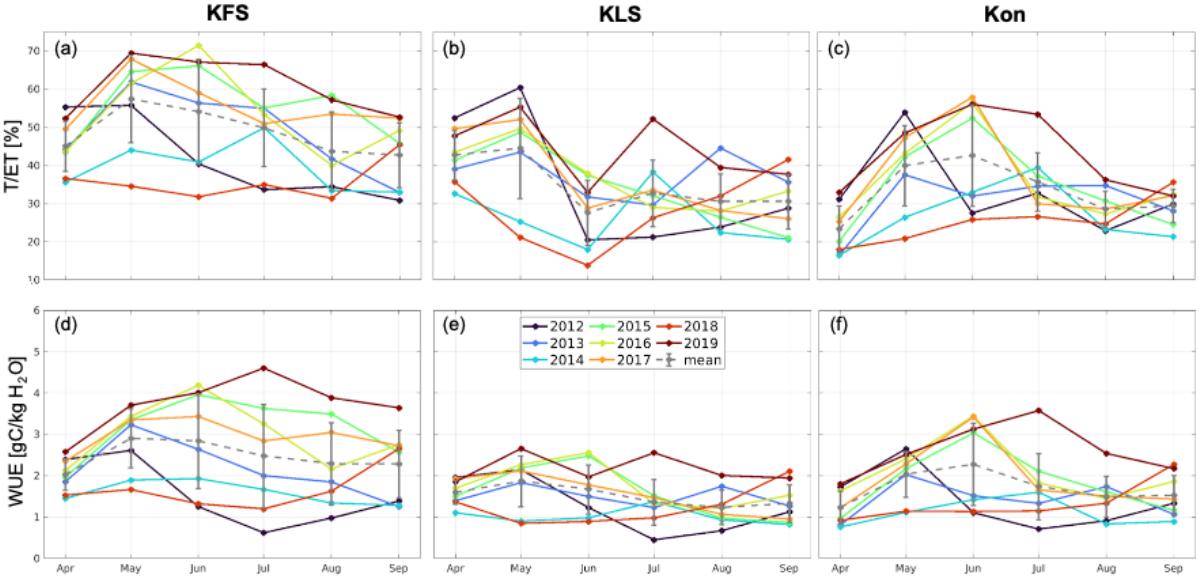

Figure 12. 2012-2019 growing season time series transpiration as a fraction of ET (a-c) and WUE (d-f) for all three study sites.

https://doi.org/10.5194/hess-2023-146
Preprint. Discussion started: 11 July 2023


Hydrology and Earth System Sciences
Discussions

Future studies would benefit from improved estimates of root water uptake since it is directly linked to the amount of available water for transpiration. Vegetation types have distinct root characteristics leading to differences in hydraulic tendencies under variable water regimes. Species specific hydraulic strategies may differ in a single location (Liu et al., 2020) so generalization of water use by PFT in hydrologic models would represent the average tendency of vegetation to regulate water. It is also possible that the changing phenological state of root systems plays an important role in root water uptake. Thus, researchers should ensure parameterizations of plant functions are accurately representing vegetation state and heterogeneity of the study area.

We find noteworthy differences when we consider the contrasting conditions in July 2012 and 2019. During both years, minimal rainfall occurred in late June into early July, but rates of ET did not decline as much in 2019 as they did in 2012. When US-KFS received rain in July 2012, there were immediate increases in rates of ET (Figure 9). This is likely due to the size of the rain events (Figure 10 coupled with the evaporative demand of the atmosphere. It is important to examine the coupling of ET and GPP since plants transpire as they process carbon. We do not observe changes in GPP during July 2012 corresponding to the increased ET, indicating the main driver or ET during this time is the evaporation component and not transpiration. Alternatively, GPP levels off in July 2019, and does not follow the 2012 decline as a result of little rainfall. This is indicative of the vegetation remaining healthy during a period of low rainfall in a year experiencing otherwise above average rainfall. The continued carbon cycling is likely due to the soil moisture available to the plants during this time (Figure A2).

The modeled vegetation responses are likely linked to the predictive phenological responses to drought (Lowman and Barros, 2018; Cui et al., 2017). As in Lowman and Barros (2018), the modeled FPAR and LAI were directly linked to the resulting GPP. By updating phenological states using the phenology model rather than forcing phenology with remotely sensed values, we are able to capture the direct vegetation response to water availability. When more water is available, DCHM-PV simulation predicts higher values of FPAR, LAI, and thus higher values of GPP than MODIS. Decreases in phenological state due to the lack of soil water available to plants affected carbon and water exchanges, validating our third hypothesis (H3). At the onset of flash drought, DCHM-V and -PV respond faster to changes in LAI and FPAR than MODIS whose affects were also seen in differences in modeled and remotely sensed GPP (Figure 8). Moreover, regardless of the simulation, the rapidness of the change in LAI and FPAR is indicative of flash drought (Figures 5 and 6) and in agreement with (Zhang et al., 2020).

4.2 Uncertainty in Vegetation Responses

We implemented three different assimilation strategies to prepare ensemble parameters to be used in the predictive phenology routine in the DCHM-PV. The 2003-2005 period represented "average" conditions as it spanned periods of below and above average precipitation. Compared to the single year assimilation periods (WET and DRY), the uncertainty ranges in model parameters were smaller in the 3YR assimilation period. The results are consistent with (Lowman and Barros, 2018) in that uncertainty in phenology shrinks during dry periods. Daily standard deviations in LAI across simulations are approximately 0.5 m^2m^{-2} during the growing season of a wet year but shrink to values of 0.2 at the onset of flash drought and less than 0.1 during peak flash drought. The lower ensemble spread during the flash drought period corresponds with winter phenological variability when plants are dormant. Similarly, decreases in uncertainty in estimates of GPP and ET during the flash drought

https://doi.org/10.5194/hess-2023-146
Preprint. Discussion started: 11 July 2023


Hydrology and Earth System Sciences
Discussions

period fall to winter levels implying variability in plant life stage and functionality are similar in drought periods and dormant months.

The growth parameters, which drives the plant activity, were all smaller in the 3YR assimilation period for all three test sites when compared to simulations from drought and wet years. Vegetation leaf out occurs later in the simulations from the 3YR assimilations (Figures 5 and 6). However, the more notable effects of the smaller growth parameters, with regards to flash drought, can be seen through the delayed phenology responses in the 3YR assimilations compared to the WET/DRY assimilations. Across the three test sites, the FPAR and LAI decreases were slower in the simulations that used the 3YR assimilation period. The vegetation that was trained using average conditions was slower to change when faced with the abrupt decrease in water availability. Although it was an above average year for precipitation, there was little rainfall in early July 2019 at our Kansas sites. At US-KLS and US-Kon, there was a rapid decrease in LAI during this time (Figure 6d,f) with some recovery in August. Moreover, the resiliency to the abrupt change is apparent in the maintenance of season LAI and FPAR dynamics from the 3YR assimilation simulations.

Future studies should use an assimilation period encompassing multiple wetness regimes (i.e. multi year inference period) to best represent the variety and variability of climatological conditions, and because it leads to less abrupt changes to extreme stress. However, if the intent of a future study is to investigate vegetation responses to extreme events in a changing climate (Kirono et al., 2020; Pearson et al., 2013, e.g.,), it may be appropriate to use inference periods encompassing only wet or dry conditions. For example, researchers could fit parameters to a dry regime if they want to investigate how plants used to wetter conditions will function in a future regime where more drought is expected.

4.3 Kansas Site Comparisons during 2012 Flash Drought

The seasonal dynamics of FPAR, LAI, and GPP from the simulations match well against the remotely sensed observations from MODIS regardless of vegetation type. However, there are subtle differences in vegetation responses to water stress across all three sites. As seen in Figures 5 and 6, the responses to flash drought at US-KLS (cropland) and US-Kon (grassland) follow a similar trajectory throughout the growing season. The savanna at US-KFS (note - AmeriFlux classifies US-KFS as a grassland but the MODIS pixel (500m) containing US-KFS reports a savanna terrain) suggests more resilience to flash drought at first when compared to croplands and grasslands in that values of FPAR and LAI are maintained for a longer period before tapering in late June. This can also be seen in the slow reductions in GPP during May and June 2012 before reaching a minimum near the beginning of July marking stomatal closure and shift toward more isohydric behavior (Meinzer, 2002). The slower reduction, driven by the lower growth rate parameter (γ), indicates that the vegetation is responding to the initial water stress, but also maintaining some activity.

The vegetation at US-KLS and US-Kon show an earlier response to the water stress in 2012 by slowing phenology (FPAR, Figure 5; LAI, Figure 6) at the beginning of May. Both sites experience another decrease in activity by the beginning of July. These conservative strategies indicate that the vegetation is more isohydric at these locations. Interestingly, when the phenology model parameters are generated from observations from a year of above average precipitation, the vegetation responds even faster to the stress of water. It is likely that the water use characteristics defined in DCHM-PV (Lowman and Barros, 2016;

https://doi.org/10.5194/hess-2023-146
Preprint. Discussion started: 11 July 2023


Hydrology and Earth System Sciences
Discussions

Garcia-Quijano and Barros, 2005) based on PFT cause the model to be more conservative in its water use strategies. Another explanation could be the deep soil layers (1.83 m, 72 in) (Soil Survey Staff) allowing for deep root the deep soils of the Kansas Plains and to allow the model to account for deeper root water uptake (Lowman and Barros, 2016).

4.4 Implications

The coupling of the land-surface-subsurface hydrology model to the predictive phenology model allows for dynamic updates of vegetation growth states (Lowman and Barros, 2018). By updating phenology, we are able to better capture vegetation responses to water stress events through water use efficiency (Figure 11), indicating plants that transpire more are more efficient in their water use. Vegetation activity is directly linked to the coupling of the water and carbon cycling through photosynthesis (Farquhar et al., 1980) and assimilating plant phenology into land-surface models (e.g., DCHM-V or Noah-MP) can improve estimates of GPP and ET (Hosseini et al., 2022; Xu et al., 2021; Mocko et al., 2021; Kumar et al., 2019). This study allows us to investigate how vegetation responses can be used to study the effects of flash droughts on the total carbon budget. Our modeling approach permits direct comparisons of remotely sensed observations to physically derived estimates. Generally, MODIS overestimates GPP compared to EC flux tower data (Heinsch et al., 2006; Running et al., 2004) and our model underestimates MODIS and flux tower GPP during drought periods and aligns more with MODIS and flux tower estimates during high precipitation years. By explicitly considering plant tendencies, we can dynamically account for current meteorological conditions and thus use physical principles to capture vegetation-atmosphere interactions. Moving forward, improvements made to phenological states of the entire plants (i.e. root systems included) rather than just the leaf phenology might better capture water movement through plants under water stress conditions.

4.5 Limitations

Capturing phenological responses within a physically based model is not without its limitations. As we update phenological states during the DCHM-PV simulations, forced atmospheric conditions from NLDAS-2 and StageIV variables are the same as in the DCHM-V simulations. We continue to use these conditions to force the model, so it is possible that the meteorological observations are already accounting for some vegetation-atmosphere interactions. When analyzing DCHM outputs against remotely sensed and eddy covariance measurements, we are comparing data across temporal and spatial scales. For example, the DCHM takes in one value for soil texture and porosity and land cover type, and uses these values to define how water moves through soils and root systems across the 4 km grid cell. Vegetation at AmeriFlux tower sites differs from the interpolated MODIS land cover type used in the DCHM in some instances. Other challenges arise throughout the analysis with missing tower data, and data at different scales, units, and measurement locations. Here, the DCHM is operating at a 4 km grid scale, so representing vegetation as one PFT does not capture the landscape heterogeneity below the grid scale even if it does match AmeriFlux. Soil moisture measurements from SMERGE, Noah-LSM, and Ameriflux (Figures A1-A6) are all at varying depths that may differ from, but most closely align with, the soil layers we defined. We derive evapotranspiration using latent heat fluxes from AmeriFlux towers and recognize that the energy balance may not be closed in doing this (Wilson et al., 2002),

https://doi.org/10.5194/hess-2023-146
Preprint. Discussion started: 11 July 2023


Hydrology and Earth System Sciences
Discussions

while the DCHM forces energy balance closure. To get past the limitations, the ensemble Monte Carlo simulations help capture model uncertainty, incorporated throughout the results as ensemble means and standard deviations.

5 Conclusions

Changes in vegetation phenology, or growth stage, drive water use strategies and have implications on the carbon and water budgets (H3). To address how water stresses affect carbon cycling, we implemented a one-dimensional version of the DCHM-V coupled to a predictive phenology model and analyzed vegetation water use strategies during drought and non drought periods. The modeling procedure first required running the DCHM-V with phenology updates from remotely sensed observations of FPAR and LAI. In order to couple the predictive phenology model to the DCHM-V, we generated ensembles of model parameters from the outputs of the DCHM-V with concurrent meteorological conditions. We ran three simulations using three distinct assimilation periods for three different sites in Kansas. Uncertainty in model parameters and outputs is reduced when a three year assimilation period (covering net-average conditions) is used. Decreases in predicted FPAR and LAI and reductions in their uncertainty ranges aligned with periods of known flash drought. These proxies for vegetation state influence rates of ET and GPP and thus WUE as seen through the partitioning of ET and the near shutdown of transpiration and carbon assimilation (H2) during the summer of 2012 (Figure 11a), while evaporation continued in response to precipitation and atmospheric demand for water (H1). The seasonal timing of the flash drought likely had larger impacts since the rapid dry down occurred during the peak growing season (Yuan et al., 2019). The amount of available water is a major influence on vegetation activity. In this region of the United States, droughts can reduce yearly carbon assimilation by 50% compared to periods of average or above average precipitation (Figure 7a-c). This has major implications for the annual crop yield as well as the carbon uptake capacity for the grasslands and savannas that cover most of the Midwestern US. Future studies should investigate how different vegetation types change their water use strategies in response to different water stresses by focusing on (1) expanding this modeling framework to include seasonal variations in the representation of root distributions which can affect subsurface responses to water stresses and (2) exploring a wider range of plant function types and climatological regimes.

Appendix A: Additional Figures

https://doi.org/10.5194/hess-2023-146
Preprint. Discussion started: 11 July 2023

Hydrology and Earth System Sciences
Discussions
Open Access
EGU

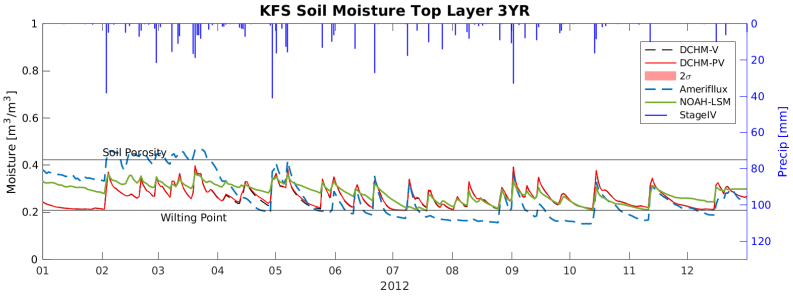

Figure A1. Top layer soil moisture at US-KFS for the flash drought year 2012.

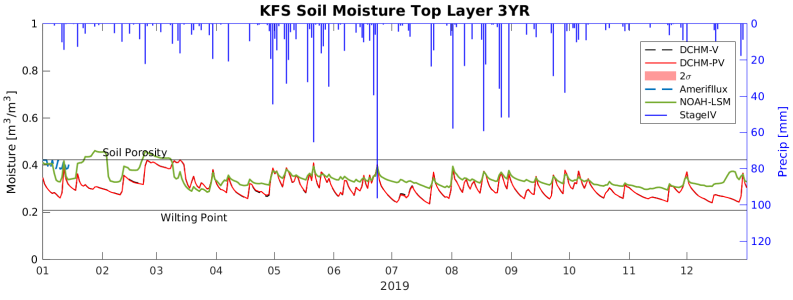

Figure A2. Top layer soil moisture for the non flash drought year 2019.

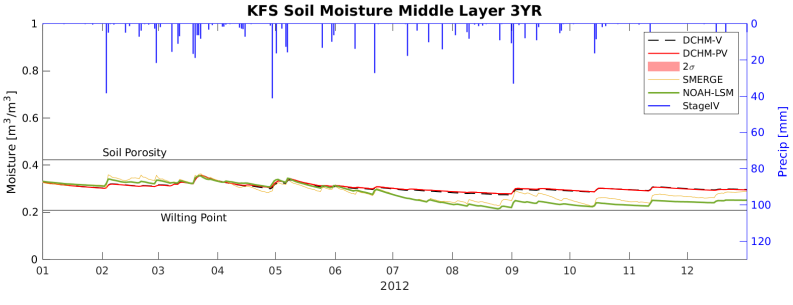

Figure A3. Middle layer soil moisture for the flash drought year 2012.

https://doi.org/10.5194/hess-2023-146
Preprint. Discussion started: 11 July 2023

Hydrology and Earth System Sciences
Discussions
Open Access
EGU

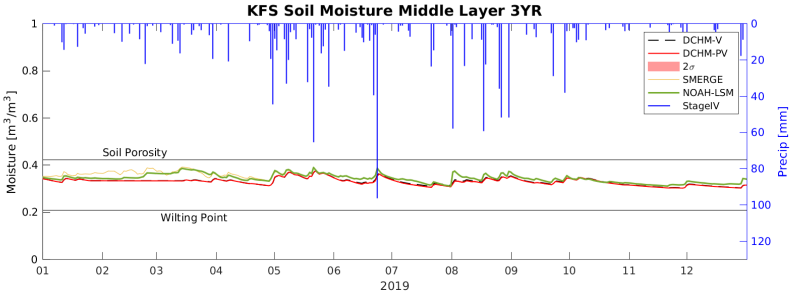

Figure A4. Middle layer soil moisture for the non flash drought year 2019.

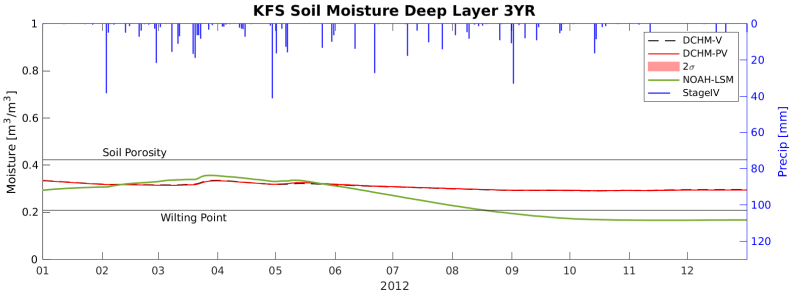

Figure A5. Deep layer soil moisture for the flash drought year 2012.

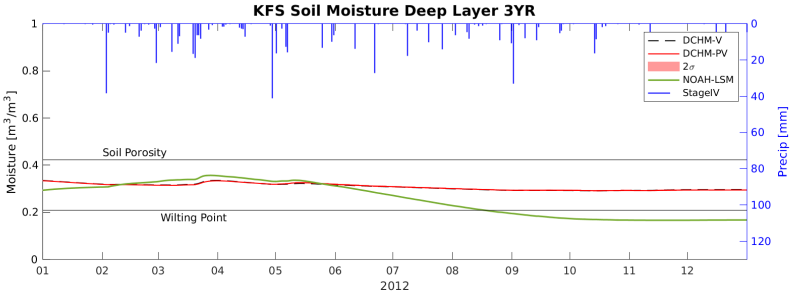

Figure A6. Deep layer soil moisture for the non flash drought year 2019.

https://doi.org/10.5194/hess-2023-146
Preprint. Discussion started: 11 July 2023

Hydrology and Earth System Sciences
Discussions

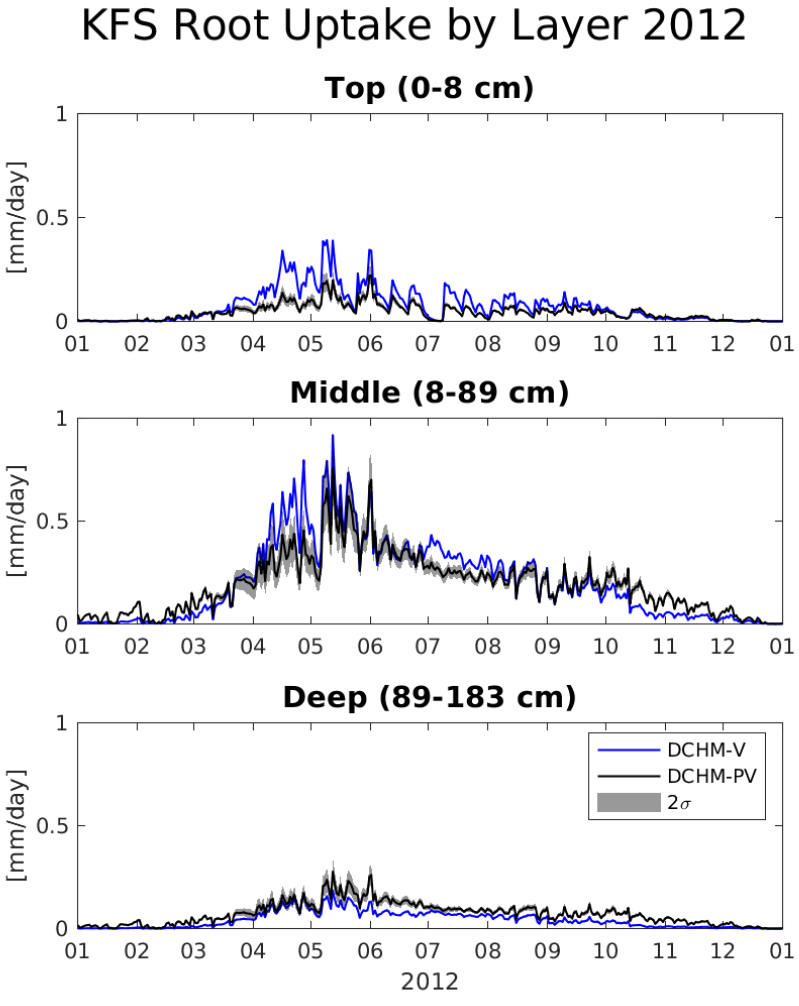

Figure A7. Root water uptake through three soil layers throughout 2012 using the DCHM-V and DCHM-PV 3YR.

https://doi.org/10.5194/hess-2023-146
Preprint. Discussion started: 11 July 2023

Hydrology and Earth System Sciences
Discussions
Open Access
EGU

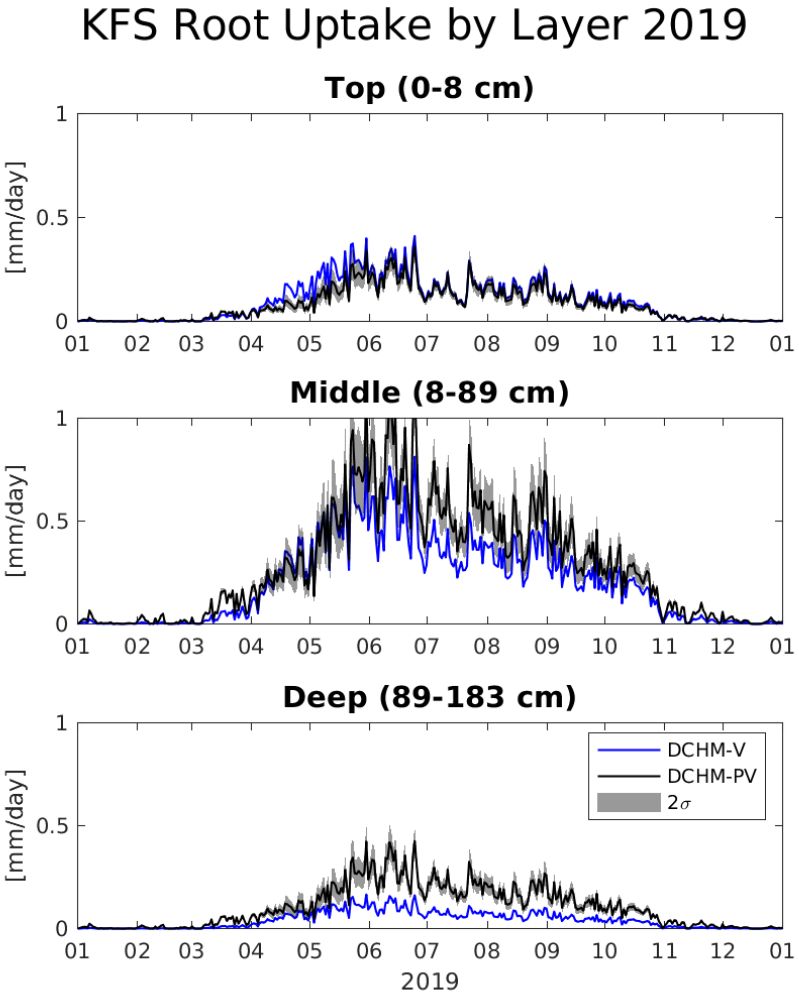

Figure A8. Root water uptake through three soil layers throughout 2019 using the DCHM-V and DCHM-PV 3YR.

https://doi.org/10.5194/hess-2023-146
Preprint. Discussion started: 11 July 2023

Hydrology and Earth System Sciences
Discussions

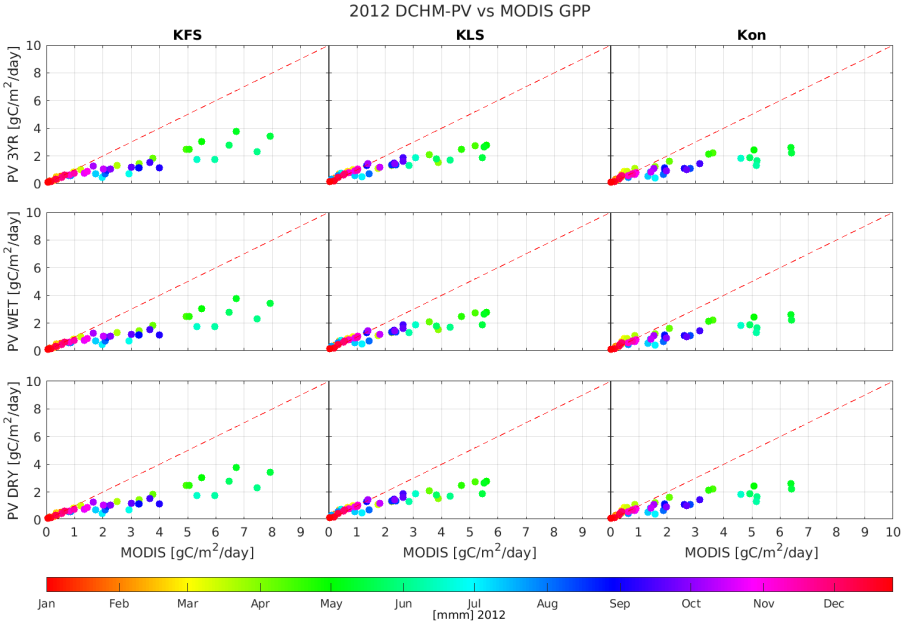

Figure A9. MODIS (MOD17A2H) vs DCHM-PV (DRY, WET, and 3YR) for all three sites during 2012.

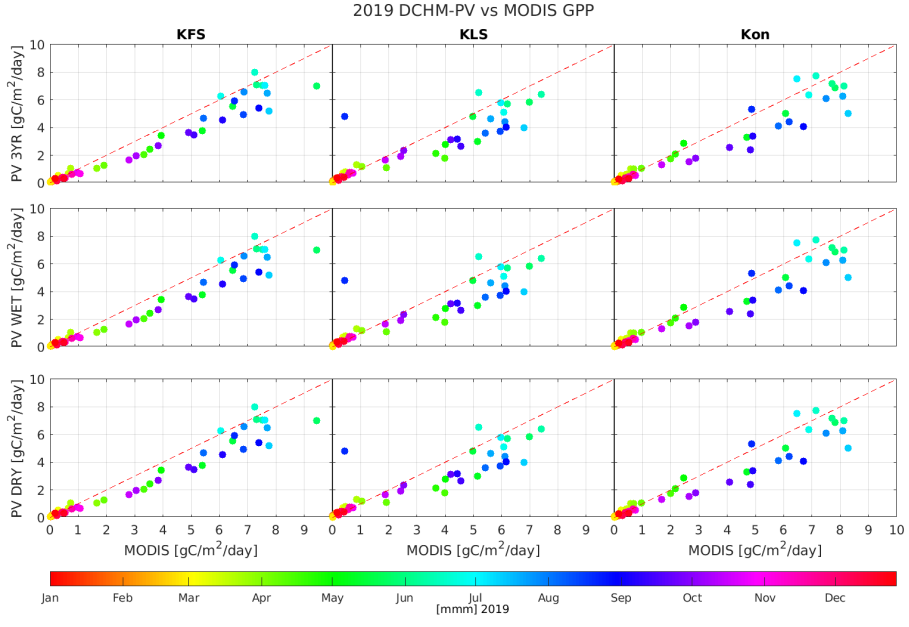

Figure A10. MODIS (MOD17A2H) vs DCHM-PV (DRY, WET, and 3YR) for all three sites during 2012.

https://doi.org/10.5194/hess-2023-146
Preprint. Discussion started: 11 July 2023

Hydrology and Earth System Sciences
Discussions
Open Access
EGU

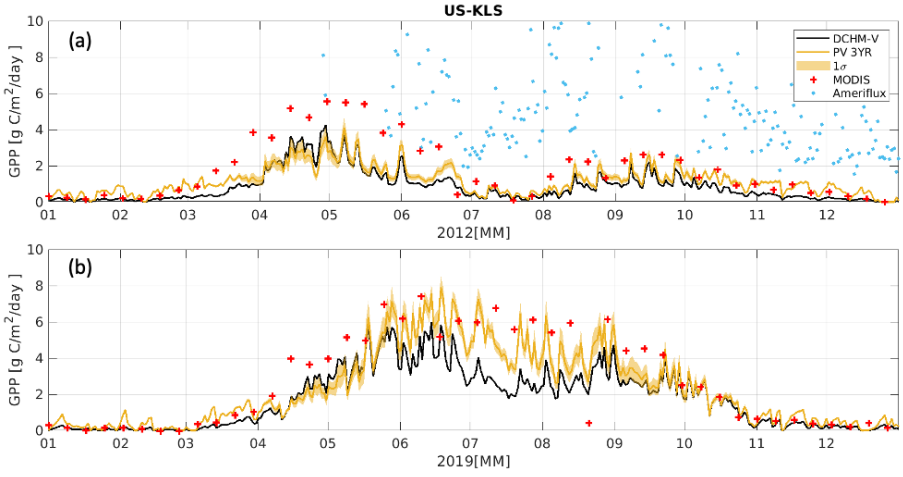

Figure A11. Time series from the DCHM-V, DCHM-PV three year assimilation period, 8 day MODIS, and daily AmeriFlux totals of GPP at US-KLS for (a) 2012, flash drought year and (b) 2019, an above average precipitation year.

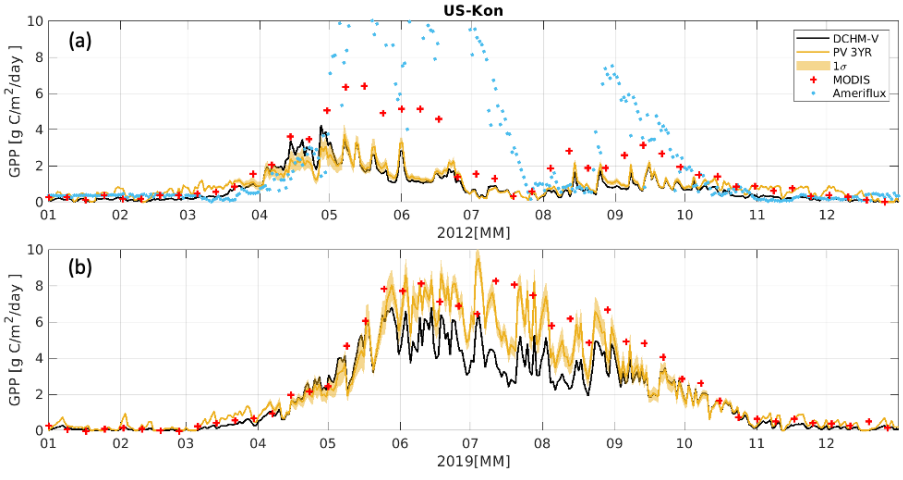

Figure A12. Time series from the DCHM-V, DCHM-PV three year assimilation period, 8 day MODIS, and daily AmeriFlux totals of GPP at US-Kon for (a) 2012, flash drought year and (b) 2019, an above average precipitation year.

https://doi.org/10.5194/hess-2023-146
Preprint. Discussion started: 11 July 2023

Hydrology and Earth System Sciences
Discussions
Open Access
EGU

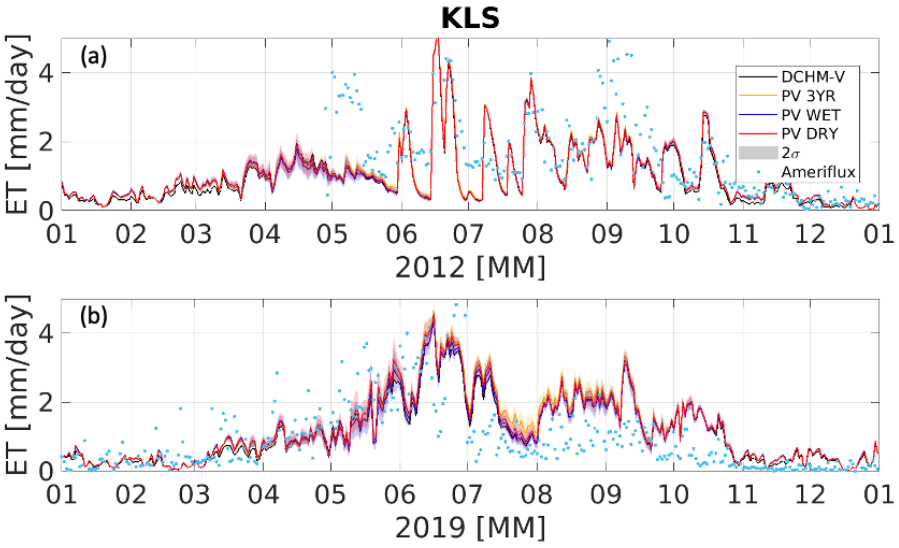

Figure A13. Time series of ET at US-KLS for (a) 2012, flash drought year and (b) 2019, wet year from DCHM-V and three different DCHM-PV simulations. Two standard deviations are shown for DCHM-PV simulations. AmeriFlux ET is showing with the blue markers.

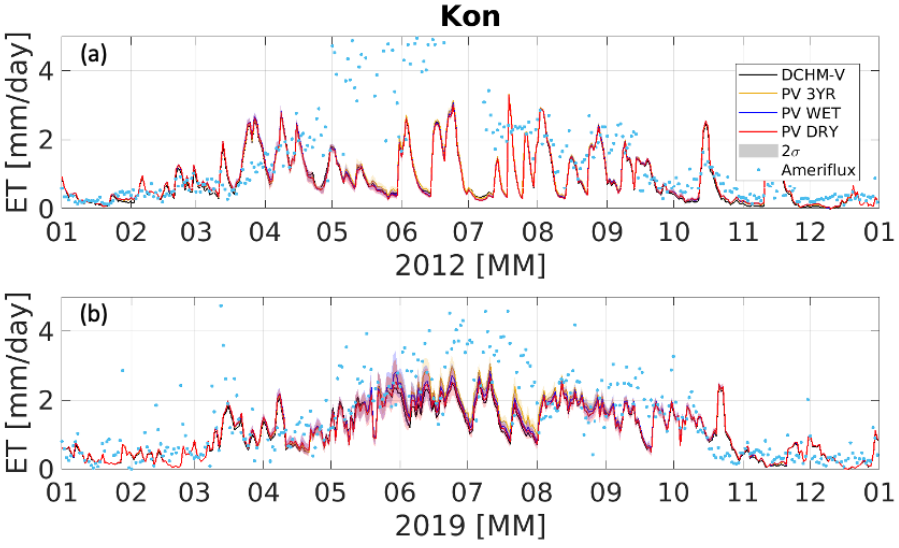

Figure A14. Time series of ET at US-Kon for (a) 2012, flash drought year and (b) 2019, wet year from DCHM-V and three different DCHM-PV simulations. Two standard deviations are shown for DCHM-PV simulations. AmeriFlux ET is showing with the blue markers.

https://doi.org/10.5194/hess-2023-146
Preprint. Discussion started: 11 July 2023

Hydrology and Earth System Sciences
Discussions

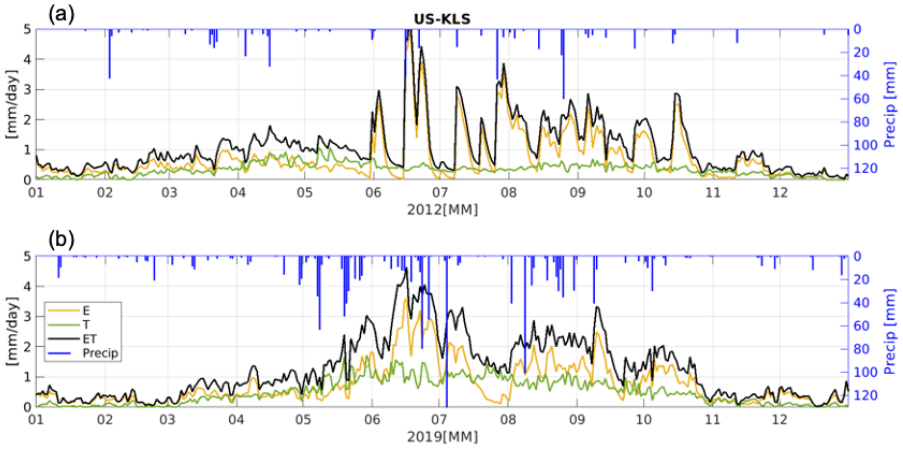

Figure A15. Simulated evapotranspiration partitioned into evaporation (E) and transpiration (T) for US-KLS in (a) 2012, flash drought and (b) 2019, wet year. Transpiration totals are in DCHM from total root uptake across the three soil layers. The top axis is daily StageIV precipitation totals.

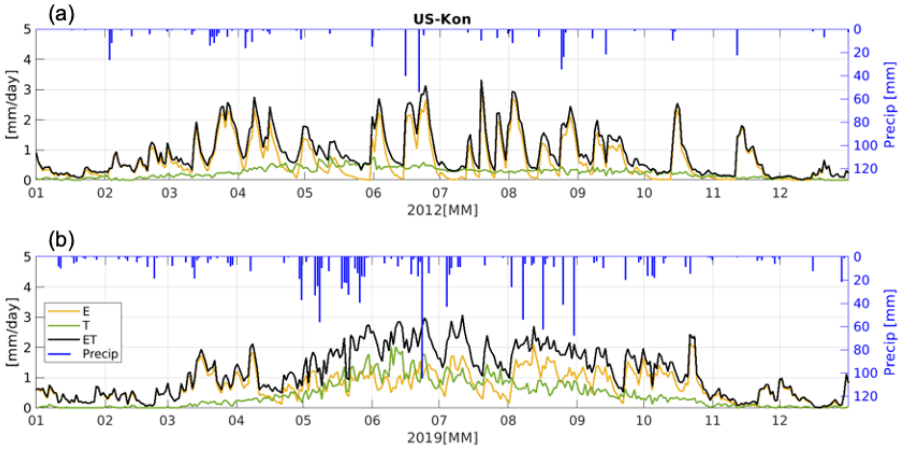

Figure A16. Simulated evapotranspiration partitioned into evaporation (E) and transpiration (T) for US-Kon in (a) 2012, flash drought and (b) 2019, wet year. Transpiration totals are in DCHM from total root uptake across the three soil layers. The top axis is daily StageIV precipitation totals.

https://doi.org/10.5194/hess-2023-146
Preprint. Discussion started: 11 July 2023

Hydrology and Earth System Sciences
Discussions

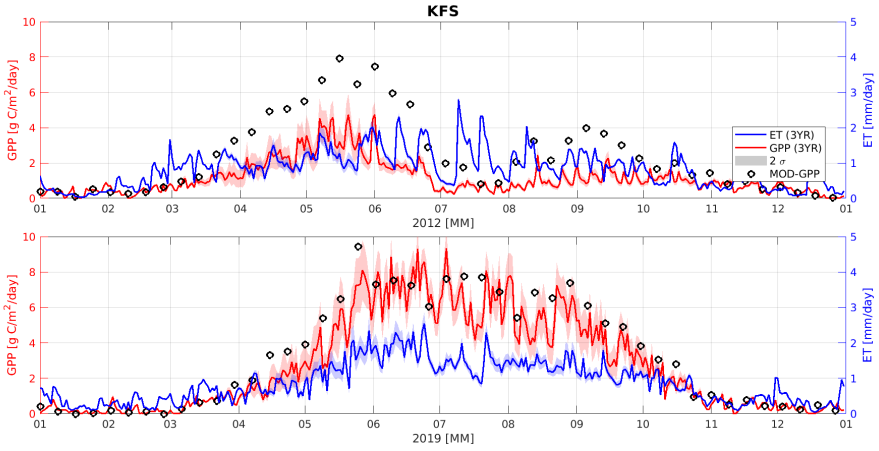

Figure A17. Simulated daily totals of GPP and ET from the DCHM-PV 3YR assimilation period for (a) 2012, flash drought year and (b) 2019, wet year.

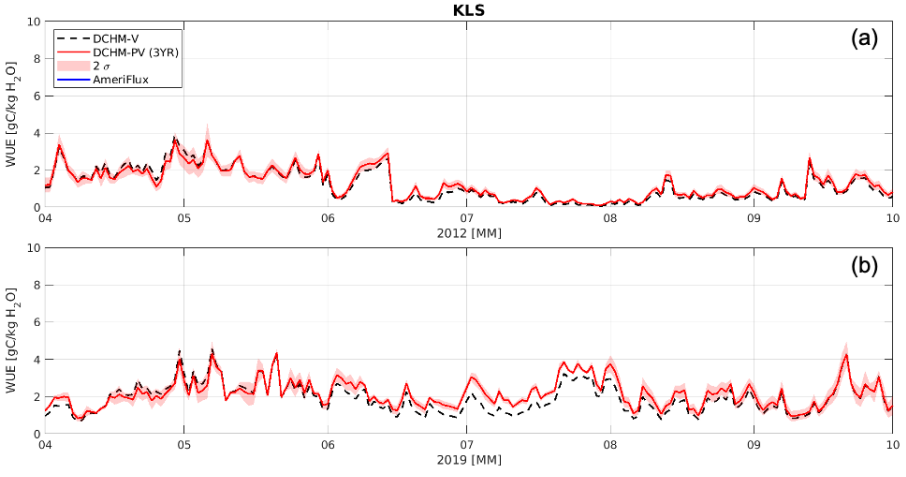

Figure A18. 2012 and 2019 water use efficiency (WUE = GPP/ET) for US-KLS.

https://doi.org/10.5194/hess-2023-146
Preprint. Discussion started: 11 July 2023

Hydrology and Earth System Sciences
Discussions
Open Access
EGU

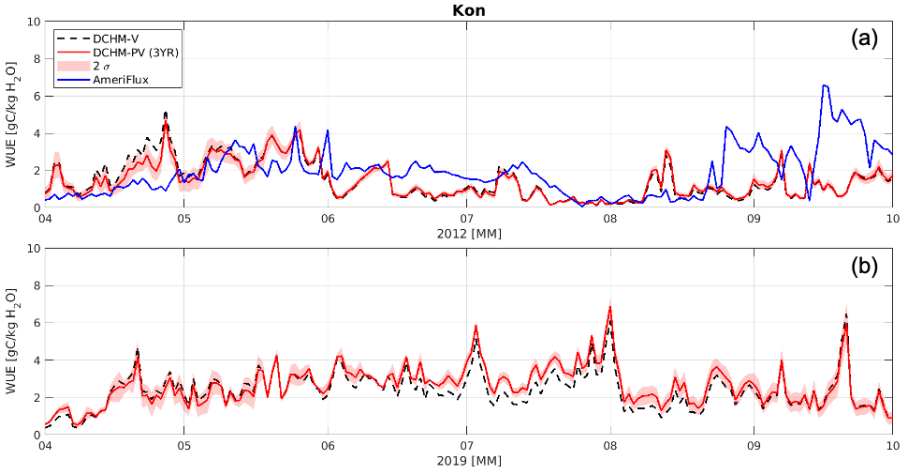

Figure A19. 2012 and 2019 water use efficiency (WUE = GPP/ET) for US-Kon.

https://doi.org/10.5194/hess-2023-146
Preprint. Discussion started: 11 July 2023


Hydrology and Earth System Sciences
Discussions

Data availability. Results from model simulations are available for download at *****.

Author contributions. TF, JO, and LL conceived the idea for this paper. LL designed the methodology and supervised implementation by NC. NC and LL analyzed results. NC wrote the original draft and prepared the submission. All authors contributed to reviewing and editing the original draft.

Competing interests. The authors declare that no competing interests exist.

Acknowledgements. The forcing data used in this study are available from a variety of sources. The NCEP/EMC Stage IV data were acquired from UCAR/NCAR - Earth Observing Laboratory and are avaiable at https://data.eol.ucar.edu/. NLDAS Phase 2, Noah-MP, and SMERGE data used in this study were acquired as part of the mission of NASA's Earth Science Division and archived and distributed by the Goddard Earth Sciences (GES) Data and Information Services Center (DISC). The MODIS MOD15A2H data were retrieved online from Appeears and distibuted by NASA Land Processes Distributed Active Archive Center (LP DAAC), http://appeears.earthdatacloud.nasa.gov/. Computations were performed using the Wake Forest University (WFU) High Performance Computing Facility, a centrally managed computational resource available to WFU researchers including faculty, staff, students, and collaborators (Information Systems and Wake Forest University, 2021). We acknowledge the following AmeriFlux sites for their data records: US-KFS, US-KLS, US-Kon. In addition, funding for AmeriFlux data resources was provided by the U.S. Department of Energy's Office of Science. were generated using data from the U.S. Drought Monitor which is jointly produced by the National Drought Mitigation Center at the University of Nebraska-Lincoln, the United States Department of Agriculture, and the National Oceanic and Atmospheric Administration.

https://doi.org/10.5194/hess-2023-146
Preprint. Discussion started: 11 July 2023

Hydrology and Earth System Sciences
Discussions

References

Baldocchi, D., Falge, E., Gu, L., Olson, R., Hollinger, D., Running, S., Anthoni, P., Bernhofer, C., Davis, K., Evans, R., et al.: FLUXNET: A new tool to study the temporal and spatial variability of ecosystem-scale carbon dioxide, water vapor, and energy flux densities, Bulletin of the American Meteorological Society, 82, 2415–2434, 2001.

Baldwin, M. and Mitchell, K.: Progress on the NCEP hourly multi-sensor US precipitation analysis for operations and GCIP research, WORLD METEOROLOGICAL ORGANIZATION-PUBLICATIONS-WMO TD, pp. 1–7, 1998.

Barros, A. P.: Adaptive multilevel modeling of land-atmosphere interactions, Journal of climate, 8, 2144–2160, 1995.

Basara, J. B., Christian, J. I., Wakefield, R. A., Otkin, J. A., Hunt, E. H., and Brown, D. P.: The evolution, propagation, and spread of flash drought in the Central United States during 2012, Environmental Research Letters, 14, 084 025, 2019.

Beer, C., Ciais, P., Reichstein, M., Baldocchi, D., Law, B., Papale, D., Soussana, J.-F., Ammann, C., Buchmann, N., Frank, D., et al.: Temporal and among-site variability of inherent water use efficiency at the ecosystem level, Global biogeochemical cycles, 23, 2009.

Brunsell, N.: AmeriFlux BASE US-KFS Kansas Field Station, Ver. 7-5, AmeriFlux AMP, (Dataset), https://doi.org/10.17190/AMF/1246132, 2020a.

Brunsell, N.: AmeriFlux BASE US-Kon Konza Prairie LTER (KNZ), Ver. 5-5, AmeriFlux AMP, (Dataset), https://doi.org/10.17190/AMF/1246068, 2020b.

Brunsell, N.: AmeriFlux BASE US-KLS Kansas Land Institute, Ver. 2-5, AmeriFlux AMP, (Dataset), https://doi.org/10.17190/AMF/1498745, 2021.

Caldararu, S., Purves, D., and Palmer, P.: Phenology as a strategy for carbon optimality: a global model, Biogeosciences, 11, 763–778, 2014.

Chen, J., Jönsson, P., Tamura, M., Gu, Z., Matsushita, B., and Eklundh, L.: A simple method for reconstructing a high-quality NDVI time-series data set based on the Savitzky–Golay filter, Remote sensing of Environment, 91, 332–344, https://doi.org/10.1016/j.rse.2004.03.014, 2004.

Chen, L., Ford, T. W., and Yadav, P.: The Role of Vegetation in Flash Drought Occurrence: A Sensitivity Study Using Community Earth System Model, Version 2, Journal of Hydrometeorology, 22, 845–857, https://doi.org/10.1175/JHM-D-20-0214.1, 2021.

Chen, L. G., Gottschalck, J., Hartman, A., Miskus, D., Tinker, R., and Artusa, A.: Flash drought characteristics based on US drought monitor, Atmosphere, 10, 498, 2019.

Christian, J. I., Basara, J. B., Lowman, L. E., Xiao, X., Mesheske, D., and Zhou, Y.: Flash drought identification from satellite-based land surface water index, Remote Sensing Applications: Society and Environment, 26, 100 770, 2022.

Christian, J. I., Minor, E. R., Basara, J. B., , Furtado, J. C., , Otkin, J. A., Lowman, L. E. L., Hunt, E. D., Mishra, V., and Xiao, X.: Global projections of flash drought show increased risk in a warming climate, Communications Earth and Environment, 4, 165, https://doi.org/10.1038/s43247-023-00826-1, 2023.

Cihlar, J., Ly, H., Li, Z., Chen, J., Pokrant, H., and Huang, F.: Multitemporal, multichannel AVHRR data sets for land biosphere studies—artifacts and corrections, Remote sensing of environment, 60, 35–57, https://doi.org/10.1016/S0034-4257(96)00137-X, 1997.

Clausnitzer, V. and Hopmans, J.: Simultaneous modeling of transient three-dimensional root growth and soil water flow, Plant and soil, 164, 299–314, 1994.

Cui, T., Martz, L., and Guo, X.: Grassland phenology response to drought in the Canadian prairies, Remote Sensing, 9, 1258, 2017.

Dai, A.: Increasing drought under global warming in observations and models, Nature climate change, 3, 52–58, 2013.

Devonec, E. and Barros, A. P.: Exploring the transferability of a land-surface hydrology model, Journal of Hydrology, 265, 258–282, 2002.

https://doi.org/10.5194/hess-2023-146
Preprint. Discussion started: 11 July 2023

Dietze, M. C.: Prediction in ecology: A first-principles framework, Ecological Applications, 27, 2048–2060, 2017.

Dietze, M. C., Lebauer, D. S., and Kooper, R.: On improving the communication between models and data, Plant, Cell & Environment, 36, 1575–1585, 2013.

Du, J.: NCEP/EMC 4KM Gridded Data (GRIB) Stage IV Data. Version 1.0, https://doi.org/10.5065/D6PG1QDD, 2011.

Farquhar, G. D. and Caemmerer, S. v.: Modelling of photosynthetic response to environmental conditions, in: Physiological plant ecology II, pp. 549–587, Springer, 1982.

Farquhar, G. D., von Caemmerer, S. v., and Berry, J. A.: A biochemical model of photosynthetic CO2 assimilation in leaves of C3 species, planta, 149, 78–90, 1980.

Ford, T. W. and Labosier, C. F.: Meteorological conditions associated with the onset of flash drought in the eastern United States, Agricultural and forest meteorology, 247, 414–423, https://doi.org/10.1016/j.agrformet.2017.08.031, 2017.

Friedl, M. and Sulla-Menashe, D.: MCD12Q1 MODIS, Terra+ Aqua Land cover type yearly L3 global 500m SIN grid, 6, 2015.

Garcia-Forner, N., Biel, C., Savé, R., and Martínez-Vilalta, J.: Isohydric species are not necessarily more carbon limited than anisohydric species during drought, Tree physiology, 37, 441–455, 2017.

Garcia-Quijano, J. F. and Barros, A. P.: Incorporating canopy physiology into a hydrological model: photosynthesis, dynamic respiration, and stomatal sensitivity, Ecological Modelling, 185, 29–49, 2005.

Gebremichael, M. and Barros, A. P.: Evaluation of MODIS gross primary productivity (GPP) in tropical monsoon regions, Remote Sensing of Environment, 100, 150–166, 2006.

Gerken, T., Bromley, G. T., Ruddell, B. L., Williams, S., and Stoy, P. C.: Convective suppression before and during the United States Northern Great Plains flash drought of 2017, Hydrology and Earth System Sciences, 22, 4155–4163, 2018.

Guo, J. S., Hultine, K. R., Koch, G. W., Kropp, H., and Ogle, K.: Temporal shifts in iso/anisohydry revealed from daily observations of plant water potential in a dominant desert shrub, New Phytologist, 225, 713–726, 2020.

He, M., Kimball, J. S., Yi, Y., Running, S., Guan, K., Jensco, K., Maxwell, B., and Maneta, M.: Impacts of the 2017 flash drought in the US Northern plains informed by satellite-based evapotranspiration and solar-induced fluorescence, Environmental Research Letters, 14, 074 019, https://doi.org/10.1088/1748-9326/ab22c3, 2019.

He, W., Ju, W., Schwalm, C. R., Sippel, S., Wu, X., He, Q., Song, L., Zhang, C., Li, J., Sitch, S., et al.: Large-scale droughts responsible for dramatic reductions of terrestrial net carbon uptake over North America in 2011 and 2012, Journal of Geophysical Research: Biogeosciences, 123, 2053–2071, https://doi.org/10.1029/2018JG004520, 2018.

Heinsch, F. A., Zhao, M., Running, S. W., Kimball, J. S., Nemani, R. R., Davis, K. J., Bolstad, P. V., Cook, B. D., Desai, A. R., Ricciuto, D. M., et al.: Evaluation of remote sensing based terrestrial productivity from MODIS using regional tower eddy flux network observations, IEEE transactions on geoscience and remote sensing, 44, 1908–1925, 2006.

Hochberg, U., Rockwell, F. E., Holbrook, N. M., and Cochard, H.: Iso/anisohydry: a plant–environment interaction rather than a simple hydraulic trait, Trends in plant science, 23, 112–120, 2018.

Hosseini, A., Mocko, D. M., Brunsell, N., Kumar, S. V., Mahanama, S. P., Arsenault, K., and Roundy, J.: Understanding the Impact of Vegetation Dynamics on the Water Cycle in the Noah-MP Model, Frontiers in Water, p. 136, 2022.

Hu, Z., Yu, G., Fu, Y., Sun, X., Li, Y., Shi, P., Wang, Y., and Zheng, Z.: Effects of vegetation control on ecosystem water use efficiency within and among four grassland ecosystems in China, Global Change Biology, 14, 1609–1619, 2008.

Hunt, E. D., Svoboda, M., Wardlow, B., Hubbard, K., Hayes, M., and Arkebauer, T.: Monitoring the effects of rapid onset of drought on non-irrigated maize with agronomic data and climate-based drought indices, Agricultural and Forest Meteorology, 191, 1–11, 2014.

https://doi.org/10.5194/hess-2023-146
Preprint. Discussion started: 11 July 2023

Information Systems and Wake Forest University: WFU High Performance Computing Facility, https://doi.org/10.57682/G13Z-2362, 2021.

Jin, C., Luo, X., Xiao, X., Dong, J., Li, X., Yang, J., and Zhao, D.: The 2012 flash drought threatened US Midwest agroecosystems, Chinese Geographical Science, 29, 768–783, https://doi.org/10.1007/s11769-019-1066-7, 2019.

Jolly, W. M., Nemani, R., and Running, S. W.: A generalized, bioclimatic index to predict foliar phenology in response to climate, Global Change Biology, 11, 619–632, 2005.

Kannenberg, S. A., Guo, J. S., Novick, K. A., Anderegg, W. R., Feng, X., Kennedy, D., Konings, A. G., Martínez-Vilalta, J., and Matheny, A. M.: Opportunities, challenges and pitfalls in characterizing plant water-use strategies, Functional Ecology, 36, 24–37, 2022.

Kim, Y., Moorcroft, P., Aleinov, I., Puma, M., and Kiang, N.: Variability of phenology and fluxes of water and carbon with observed and simulated soil moisture in the Ent Terrestrial Biosphere Model (Ent TBM version 1.0. 1.0. 0), Geoscientific Model Development, 8, 3837–3865, 2015.

Kimball, J. S., Jones, L., Jensco, K., He, M., Maneta, M., and Reichle, R.: SMAP L4 assessment of the US northern plains 2017 flash drought, in: IGARSS 2019-2019 IEEE International Geoscience and Remote Sensing Symposium, pp. 5366–5369, IEEE, 2019.

Kirono, D. G., Round, V., Heady, C., Chiew, F. H., and Osbrough, S.: Drought projections for Australia: Updated results and analysis of model simulations, Weather and Climate Extremes, 30, 100 280, 2020.

Konings, A. G. and Gentine, P.: Global variations in ecosystem-scale isohydricity, Global change biology, 23, 891–905, 2017.

Kumar, S. V., Mocko, D. M., Wang, S., Peters-Lidard, C. D., and Borak, J.: Assimilation of remotely sensed leaf area index into the Noah-MP land surface model: Impacts on water and carbon fluxes and states over the continental United States, Journal of Hydrometeorology, 20, 1359–1377, 2019.

Lai, C.-T. and Katul, G.: The dynamic role of root-water uptake in coupling potential to actual transpiration, Advances in Water Resources, 23, 427–439, 2000.

Li, L., Yang, Z.-L., Matheny, A. M., Zheng, H., Swenson, S. C., Lawrence, D. M., Barlage, M., Yan, B., McDowell, N. G., and Leung, L. R.: Representation of plant hydraulics in the Noah-MP land surface model: Model development and multiscale evaluation, Journal of Advances in Modeling Earth Systems, 13, e2020MS002 214, 2021.

Lisonbee, J., Woloszyn, M., and Skumanich, M.: Making sense of flash drought: Definitions, indicators, and where we go from here, J. Appl. Serv. Climatol, 2021, 1–19, https://doi.org/10.46275/JOASC.2021.02.001, 2021.

Liu, Y., Kumar, M., Katul, G. G., Feng, X., and Konings, A. G.: Plant hydraulics accentuates the effect of atmospheric moisture stress on transpiration, Nature Climate Change, 10, 691–695, 2020.

Lowman, L. E. and Barros, A. P.: Interplay of drought and tropical cyclone activity in SE US gross primary productivity, Journal of Geophysical Research: Biogeosciences, 121, 1540–1567, https://doi.org/10.1002/2015JG003279, 2016.

Lowman, L. E. and Barros, A. P.: Predicting canopy biophysical properties and sensitivity of plant carbon uptake to water limitations with a coupled eco-hydrological framework, Ecological Modelling, 372, 33–52, 2018.

Lowman, L. L., Christian, J. I., and Hunt, E. D.: How land surface characteristics influence the development of flash drought through the drivers of soil moisture and vapor pressure deficit, Journal of Hydrometeorology, https://doi.org/10.1175/JHM-D-22-0158.1, in press.

Meinzer, F. C.: Co-ordination of vapour and liquid phase water transport properties in plants, Plant, Cell & Environment, 25, 265–274, 2002.

Miller, D. A. and White, R. A.: A conterminous United States multilayer soil characteristics dataset for regional climate and hydrology modeling, Earth interactions, 2, 1–26, 1998.

https://doi.org/10.5194/hess-2023-146
Preprint. Discussion started: 11 July 2023

Mitchell, K. E., Lohmann, D., Houser, P. R., Wood, E. F., Schaake, J. C., Robock, A., Cosgrove, B. A., Sheffield, J., Duan, Q., Luo, L., et al.: The multi-institution North American Land Data Assimilation System (NLDAS): Utilizing multiple GCIP products and partners in a continental distributed hydrological modeling system, Journal of Geophysical Research: Atmospheres, 109, 2004.

Mocko, D. M., Kumar, S. V., Peters-Lidard, C. D., and Wang, S.: Assimilation of vegetation conditions improves the representation of drought over agricultural areas, Journal of Hydrometeorology, 22, 1085–1098, 2021.

Moradkhani, H., Sorooshian, S., Gupta, H. V., and Houser, P. R.: Dual state–parameter estimation of hydrological models using ensemble Kalman filter, Advances in water resources, 28, 135–147, https://doi.org/10.1016/j.advwatres.2004.09.002, 2005.

Myneni, R., Knyazikhin, Y., and Park, T.: MOD15A2H MODIS/Terra leaf area Index/FPAR 8-Day L4 global 500m SIN grid V006, NASA EOSDIS Land Processes DAAC, 2015.

Novick, K. A., Ficklin, D. L., Stoy, P. C., Williams, C. A., Bohrer, G., Oishi, A. C., Papuga, S. A., Blanken, P. D., Noormets, A., Sulman, B. N., et al.: The increasing importance of atmospheric demand for ecosystem water and carbon fluxes, Nature climate change, 6, 1023–1027, 2016.

Otkin, J. A., Anderson, M. C., Hain, C., Svoboda, M., Johnson, D., Mueller, R., Tadesse, T., Wardlow, B., and Brown, J.: Assessing the evolution of soil moisture and vegetation conditions during the 2012 United States flash drought, Agricultural and forest meteorology, 218, 230–242, https://doi.org/10.1016/j.agrformet.2015.12.065, 2016.

Otkin, J. A., Svoboda, M., Hunt, E. D., Ford, T. W., Anderson, M. C., Hain, C., and Basara, J. B.: Flash droughts: A review and assessment of the challenges imposed by rapid-onset droughts in the United States, Bulletin of the American Meteorological Society, 99, 911–919, https://doi.org/10.1175/BAMS-D-17-0149.1, 2018.

Otkin, J. A., Woloszyn, M., Wang, H., Svoboda, M., Skumanich, M., Pulwarty, R., Lisonbee, J., Hoell, A., Hobbins, M., Haigh, T., et al.: Getting ahead of Flash Drought: From Early Warning to Early Action, Bulletin of the American Meteorological Society, 103, E2188–E2202, 2022.

Pearson, R. G., Phillips, S. J., Loranty, M. M., Beck, P. S., Damoulas, T., Knight, S. J., and Goetz, S. J.: Shifts in Arctic vegetation and associated feedbacks under climate change, Nature climate change, 3, 673–677, 2013.

Poonia, V., Goyal, M. K., Jha, S., and Dubey, S.: Terrestrial ecosystem response to flash droughts over India, Journal of Hydrology, 605, 127 402, 2022.

Qing, Y., Wang, S., Ancell, B. C., and Yang, Z.-L.: Accelerating flash droughts induced by the joint influence of soil moisture depletion and atmospheric aridity, Nature communications, 13, 1–10, 2022.

Roman, D., Novick, K., Brzostek, E., Dragoni, D., Rahman, F., and Phillips, R.: The role of isohydric and anisohydric species in determining ecosystem-scale response to severe drought, Oecologia, 179, 641–654, 2015.

Running, S., Mu, Q., and Zhao, M.: MOD17A2H MODIS/terra gross primary productivity 8-day L4 global 500m SIN grid V006, NASA EOSDIS Land Processes DAAC, 2015.

Running, S. W., Nemani, R. R., Heinsch, F. A., Zhao, M., Reeves, M., and Hashimoto, H.: A continuous satellite-derived measure of global terrestrial primary production, Bioscience, 54, 547–560, 2004.

Sade, N., Gebremedhin, A., and Moshelion, M.: Risk-taking plants: anisohydric behavior as a stress-resistance trait, Plant signaling & behavior, 7, 767–770, 2012.

Savitzky, A. and Golay, M. J.: Smoothing and differentiation of data by simplified least squares procedures., Analytical chemistry, 36, 1627–1639, 1964.

https://doi.org/10.5194/hess-2023-146
Preprint. Discussion started: 11 July 2023

Soil Survey Staff, Natural Resources Conservation Service, U. S. D. o. A.: Web Soil Survey. Available online. Accessed 07 December 2022, https://www.nrcs.usda.gov/resources/data-and-reports/web-soil-survey.

Stöckli, R., Rutishauser, T., Dragoni, D., O'keefe, J., Thornton, P., Jolly, M., Lu, L., and Denning, A.: Remote sensing data assimilation for a prognostic phenology model, Journal of Geophysical Research: Biogeosciences, 113, https://doi.org/10.1029/2008JG000781, 2008.

Sulla-Menashe, D. and Friedl, M. A.: User guide to collection 6 MODIS land cover (MCD12Q1 and MCD12C1) product, USGS: Reston, VA, USA, 1, 18, 2018.

Svoboda, M., LeComte, D., Hayes, M., Heim, R., Gleason, K., Angel, J., Rippey, B., Tinker, R., Palecki, M., Stooksbury, D., et al.: The drought monitor, Bulletin of the American Meteorological Society, 83, 1181–1190, 2002.

Tanré, D., Kaufman, Y., Herman, M., and Mattoo, S.: Remote sensing of aerosol properties over oceans using the MODIS/EOS spectral radiances, Journal of Geophysical Research: Atmospheres, 102, 16 971–16 988, https://doi.org/10.1029/96JD03437, 1997.

Tao, J. and Barros, A.: Coupled prediction of flood response and debris flow initiation during warm-and cold-season events in the Southern Appalachians, USA, Hydrology and Earth System Sciences, 18, 367–388, 2014.

Tao, J. and Barros, A. P.: Prospects for flash flood forecasting in mountainous regions–An investigation of Tropical Storm Fay in the Southern Appalachians, Journal of Hydrology, 506, 69–89, 2013.

Tobin, K. J., Bennett, M. E., and Torres, R.: Long-term root zone moisture trends across CONUS from a new root-zone soil moisture product called SMERGE, in: AGU Fall Meeting Abstracts, vol. 2019, pp. H51S–1750, 2019.

Trenberth, K. E., Dai, A., Van Der Schrier, G., Jones, P. D., Barichivich, J., Briffa, K. R., and Sheffield, J.: Global warming and changes in drought, Nature Climate Change, 4, 17–22, 2014.

Wilson, K., Goldstein, A., Falge, E., Aubinet, M., Baldocchi, D., Berbigier, P., Bernhofer, C., Ceulemans, R., Dolman, H., Field, C., et al.: Energy balance closure at FLUXNET sites, Agricultural and Forest Meteorology, 113, 223–243, 2002.

Wu, G., Guan, K., Li, Y., Novick, K. A., Feng, X., McDowell, N. G., Konings, A. G., Thompson, S. E., Kimball, J. S., De Kauwe, M. G., et al.: Interannual variability of ecosystem iso/anisohydry is regulated by environmental dryness, New Phytologist, 229, 2562–2575, 2021.

Xia, Y., Mitchell, K., Ek, M., Sheffield, J., Cosgrove, B., Wood, E., Luo, L., Alonge, C., Wei, H., Meng, J., et al.: Continental-scale water and energy flux analysis and validation for the North American Land Data Assimilation System project phase 2 (NLDAS-2): 1. Intercomparison and application of model products, Journal of Geophysical Research: Atmospheres, 117, 2012.

Xu, T., Chen, F., He, X., Barlage, M., Zhang, Z., Liu, S., and He, X.: Improve the performance of the noah-MP-crop model by jointly assimilating soil moisture and vegetation phenology data, Journal of Advances in Modeling Earth Systems, 13, e2020MS002 394, 2021.

Yao, T., Liu, S., Hu, S., and Mo, X.: Response of vegetation ecosystems to flash drought with solar-induced chlorophyll fluorescence over the Hai River Basin, China during 2001–2019, Journal of Environmental Management, 313, 114 947, 2022.

Yildiz, O. and Barros, A. P.: Climate variability, water resources, and hydrologic extremes—Modeling the water and energy budgets, Climate and Hydrology, in Mountain Areas, pp. 291–306, 2005.

Yildiz, O. and Barros, A. P.: Elucidating vegetation controls on the hydroclimatology of a mid-latitude basin, Journal of Hydrology, 333, 431–448, 2007.

Yuan, X., Wang, L., Wu, P., Ji, P., Sheffield, J., and Zhang, M.: Anthropogenic shift towards higher risk of flash drought over China, Nature communications, 10, 1–8, 2019.

Zeng, X.: Global vegetation root distribution for land modeling, Journal of Hydrometeorology, 2, 525–530, 2001.

Zhang, M. and Yuan, X.: Rapid reduction in ecosystem productivity caused by flash droughts based on decade-long FLUXNET observations, Hydrology and Earth System Sciences, 24, 5579–5593, 2020.

https://doi.org/10.5194/hess-2023-146
Preprint. Discussion started: 11 July 2023

705 Zhang, M., Yuan, X., and Otkin, J. A.: Remote sensing of the impact of flash drought events on terrestrial carbon dynamics over China, Carbon Balance and Management, 15, 1–11, https://doi.org/10.1186/s13021-020-00156-1, 2020.

Zhou, S., Duursma, R. A., Medlyn, B. E., Kelly, J. W., and Prentice, I. C.: How should we model plant responses to drought? An analysis of stomatal and non-stomatal responses to water stress, Agricultural and Forest Meteorology, 182, 204–214, 2013.